Buletin Ilmiah Sarjana Teknik Elektro
Vol. 8, No. 6, December 2026, pp. 1789-1816
ISSN: 2685-9572, DOI: 10.12928/biste.v8i6.17384

Internet of Things-Enabled Edge–Cloud Digital Twin and Network-Aware Predictive Control for Anomaly-Resilient PV–Battery Microgrids

Ammar Dawood Jasim [1], **Zaid Shafeeq Bakr** [2], **Mohammed Al-Daloo** [3], **Mas Al-Qutbi** [4]
[1] Department of Computer Networks Engineering, College of Information Engineering, Al-Nahrain University, Jadriya, Baghdad, Iraq
[2] Department of Automation and Artificial Intelligence Engineering, College of Information Engineering, Al-Nahrain University, Jadriya, Baghdad, Iraq
[3] Department of Communications and Information Engineering, College of Information Engineering, Al-Nahrain University, Jadriya, Baghdad, Iraq
[4] Department of Medical Physics, University of Kut, College of Science, Wasit, Iraq

ARTICLE INFORMATION

Article History:

Received 06 July 2026
Revised 17 October 2026
Accepted 23 November 2026

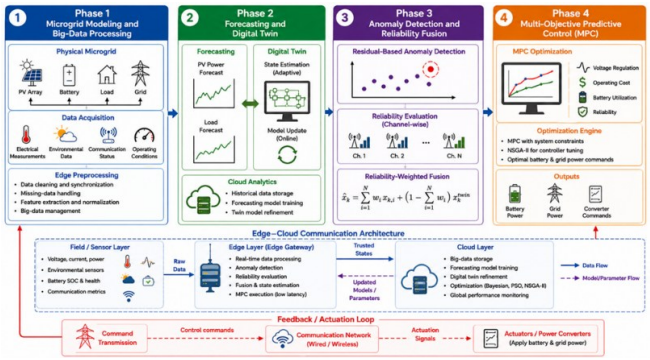
Keywords:

Artificial Intelligence;
Digital Twin;
Edge–Cloud Computing;
Internet of Things (IoT);
Model Predictive Control

Corresponding Author:
Mas Al-Qutbi,
Department of Medical Physics, University of Kut, College of Science, Wasit, Iraq.
Email:
mass.khudhair@alkutcollege.edu.iq

This work is open access under a Creative Commons Attribution-Share Alike 4.0

ABSTRACT



This paper presents an Artificial Intelligence (AI)-driven big-data digital-twin framework with network-aware Model Predictive Control (MPC) for anomaly-resilient PV–battery microgrids. The proposed system adopts an IoT-enabled edge–cloud architecture in which distributed sensors, battery-management units, converter actuators, an edge gateway, cloud resources, and the supervisory controller exchange measurements and control commands through bidirectional communication channels. Electrical, environmental, battery, and network-status data are processed at the edge, while the cloud supports data storage, forecasting-model training, digital-twin refinement, and optimization. Bayesian optimization is used for PV/load forecasting, particle swarm optimization for anomaly-detector tuning, and NSGA-II for multi-objective MPC parameter selection. Channel-wise reliability-weighted fusion combines physical measurements with digital-twin estimates to construct trusted controller states. The framework was evaluated under nominal, cloud–load, False-Data-Injection (FDI), and mixed cyber-physical anomaly conditions against four baseline controllers. It achieved the lowest aggregate voltage RMSE of 1.561V, corresponding to reductions of 22.57–51.28%. Under FDI, the RMSE decreased to 0.843V with a recall of 0.959, while under mixed anomalies it reached 2.674V with an F1-score of 0.684. Although PV forecasting accuracy was limited during rapid irradiance variations, the strongest improvements occurred when measurement integrity was degraded, indicating that resilience is mainly provided by reliability-weighted digital-twin fusion. The framework also achieved a 95th-percentile edge-processing latency of 2.422ms with approximately 99.86% solver success, supporting low-latency edge execution while leaving end-to-end network performance for future validation.

Document Citation:

A. D. Jasim, Z. S. Bakr, M. Al-Daloo, and M. Al-Qutbi, "Internet of Things-Enabled Edge–Cloud Digital Twin and Network-Aware Predictive Control for Anomaly-Resilient PV–Battery Microgrids," *Buletin Ilmiah Sarjana Teknik Elektro*, vol. 8, no. 6, pp. 1789-1816, 2026, DOI: 10.12928/biste.v8i6.17384.

1. INTRODUCTION

The increasing demand for sustainable, reliable, and low-carbon energy systems has accelerated the development of microgrids as an effective solution for integrating distributed renewable generation, energy-storage systems, controllable loads, and utility-grid support within a coordinated local energy environment. A microgrid can operate in either grid-connected or islanded mode and manage its available resources according to technical, economic, and operational requirements [1]. Through coordinated control of generation, storage, and demand, microgrids can improve local energy flexibility, reduce dependence on centralized generation, and support more efficient use of renewable resources. This flexibility makes microgrids particularly suitable for residential, commercial, industrial, and remote applications, where continuity of supply, improved renewable-energy utilization, enhanced power quality, and efficient local energy management are essential. In addition, the increasing use of digital monitoring, distributed sensors, intelligent controllers, and the communication-enabled applainces is transforming modern microgrids into highly interconnected cyber-physical systems in which reliable information exchange is becoming increasingly important for coordinated operation [2].

As illustrated in Figure 1, an intelligent microgrid combines distributed energy sources, battery storage, alternating-current and direct-current buses, local loads, an energy-management system, power converters, communication infrastructure, and a supervisory controller. These components interact through coordinated power and information flows to support real-time monitoring, optimization, and control. This architecture for an electro-mechanical system, however, creates additional dependency on precise sensor readings, quick communications, secure data exchange, and effective control actions. Thus, any disturbance in the electrical network or the communications network can spread to the control loop and influence the performance of the system [3] .

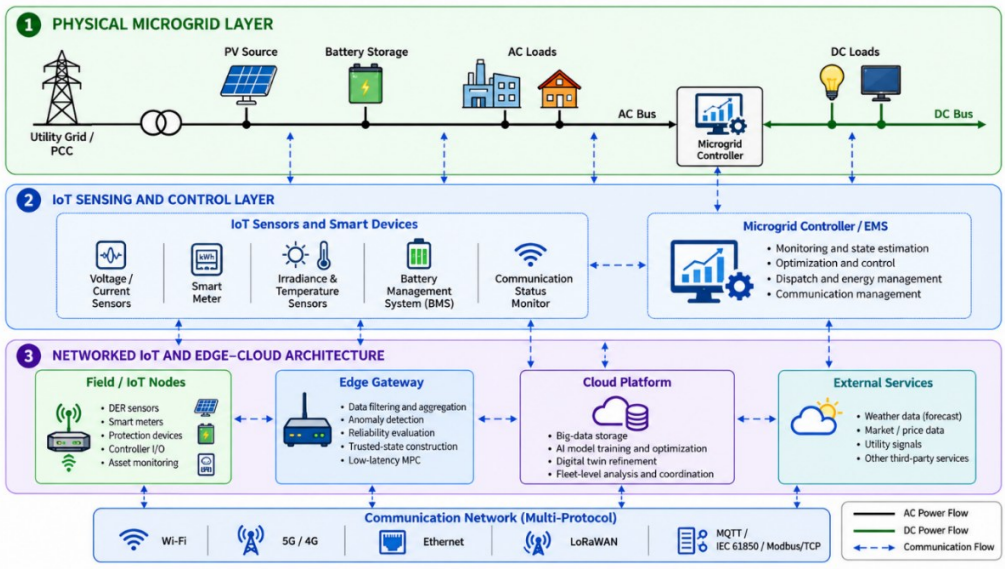


Figure 1. General architecture of an intelligent microgrid

There is considerable uncertainty associated with renewable energy sources due to varying outputs dependent on environmental and operational conditions. Photovoltaic (PV) output depends greatly on irradiance levels, temperature, cloud movements, and partial shadowing, whereas the electrical load depends on user activity, consumption pattern and sudden load occurrences [4]. Discrepancy between these two will cause voltage variations of DC bus, inefficient conversion of grid power, stress on converters and frequent battery cycling. Battery energy storage is thus necessary to store excess PV generation and to compensate for any lack of PV generation. However, the battery storage state-of-charge should be maintained within the permissible operating range to prevent rapid degradation and increased failure rate [5].

Rule-based and proportional-integral controllers have been extensively used in microgrid systems due to their simplicity in design and implementation, as well as low computational demands. Controllers can perform satisfactorily when operating under steady-state or slowly changing conditions. Nevertheless, fixed control laws and constant gains employed by rule-based and proportional-integral controllers may prevent them from being able to adequately adapt to the dynamic nature of the system in terms of PV-battery microgrids in

particular and with regard to fast-changing irradiance, sudden changes in load, uncertainties, interferences in communication, and distorted measurements. However, MPC becomes a more flexible approach in the considered application because it makes the forecast of future dynamics and determines the sequence of optimal control moves taking into account constraints related to voltage, power, converters, grid, batteries, and others. Also, as a predictive controller, it provides the possibility to solve a multi-objective control problem at once. Nevertheless, it is necessary to point out that the performance of the predictive controller substantially relies on accurate model predictions, disturbances predictions, and quality measurements with prompt access to them. As a result, incorrect predictions, uncertainty of models, loss of packets, and bad quality of measurements will deteriorate the predictive control performance [6].

The extensive deployment of smart meters, Internet of Things (IoT) devices, environmental sensors, battery-management units, converter-monitoring systems, and communication nodes has transformed microgrids into data-intensive platforms. These systems continuously generate heterogeneous streams of voltage, current, power, irradiance, temperature, load, battery, controller, and network information. Such data exhibit the principal characteristics of big data, including high volume, velocity, variety, and veracity requirements. In particular, data veracity is critical because delayed, missing, replayed, or deliberately manipulated measurements may appear physically plausible while producing unsuitable control actions. Therefore, big-data management in intelligent microgrids must extend beyond data storage and include synchronization, cleaning, missing-data handling, feature extraction, reliability assessment, and low-latency decision support [7][8].

A communication system between the edge and the cloud provides a very efficient way of deploying the computational capabilities mentioned above. In the edge layer, time-sensitive calculations like signal pre-processing, residual calculation, abnormality detection, reliability assessment, state estimation, and MPC implementation can be executed near the actual physical systems. On the other hand, the cloud layer can offer functionalities like history data storage, training of artificial intelligence models, improving the digital twin, optimization, and monitoring of performance. However, the two-way communications between the sensors, edge layer, cloud resources, controllers, and power converters are vulnerable to packet loss, communication latency, replay attack, and false-data injection [9].

The digital-twin approach offers a connection between the physical microgrid and its virtual counterpart in a dynamic fashion. The digital twin is capable of replicating system dynamics, estimating unknown system states, predicting future system behavior, testing controllers, and providing an alternative data source for when the physical measurement becomes unreliable or corrupt. The digital twin, once in sync with the physical system, can contribute towards enhancing the state information and resilience of control algorithms. However, it can be unadvisable to be overly reliant on virtual estimation since modeling errors and parameter uncertainties could cause the accuracy of the twins to decrease especially in case of quick changes of PV and loads [10].

Cyber-physical errors such as sensing bias, False Data Injection (FDI), packet drops, retransmission attacks, delays, and model mismatch can have an adverse effect on microgrids' operations. The control system can misinterpret the erroneous feedback information as a true physical event and act accordingly, sending wrong instructions about battery power or grid power. The reliable operation demands that not only do we detect anomalies but also develop a way to evaluate how the reliable each feedback measurement is before feeding it into the control loop. Channel-wise reliability assessment can be achieved through the comparison of physical measurements with the estimates from the digital twin, with a gradual reduction in weight of doubtful data [11].

Furthermore, Artificial intelligence (AI) has the potential for better forecasting of renewable energy sources, load prediction, anomalies, state estimation, and controller tuning. Nevertheless, the success of such AI methods depends greatly on the choice of parameters and hyperparameters used. This is why optimization algorithms are needed to synchronize all learning and control parts.Bayesian optimization is suitable for tuning forecasting models whose evaluation involves repeated training and validation, particle swarm optimization (PSO) can adjust nonlinear anomaly-detector parameters, and the non-dominated sorting genetic algorithm II (NSGA-II) can identify trade-offs among conflicting control objectives such as voltage regulation, operating cost, battery utilization, and control effort. Integrating these algorithms within a unified framework enables each component to be optimized according to its specific role rather than the relying on a single general-purpose tuning procedure [12].

Despite considerable progress in intelligent microgrid research, big-data processing, AI-based forecasting, digital-twin modeling, communication-network monitoring, anomaly detection, and predictive control are frequently investigated as independent functions. Limited attention has been given to their coordinated operation within a unified network-aware closed-loop framework. This separation restricts the

ability of existing approaches to distinguish genuine physical disturbances from corrupted measurements and to maintain reliable control when communication and sensing information become uncertain [13][14].

The solution to such issues will be presented in the form of a reliability-weighted digital-twin MPC system that would provide resilience against anomalies for PV-battery microgrids in the edge–cloud environment powered by IoT technologies. The unique feature of the proposed approach is the incorporation of the measurement reliability in the closed-loop control loop. The approach does not require treating the problem of anomaly detection as an additional supervisory process or making an accept/reject decision about the measured values. The physical measurements are continuously integrated with their digital-twin estimates depending on their reliability. This allows the unreliable measurements to be assigned less importance without necessarily ignoring any physically meaningful data when the sensor is partially unreliable. The update mechanism of the digital twin adaptation algorithm is also governed by reliability constraints in order to minimize the likelihood of using unreliable measurements for the virtual model update. Furthermore, the proposed approach incorporates Bayesian-optimized photovoltaic and load forecasting, particle swarm optimization-based tuning of the anomaly detector, and multi-objective MPC controller design using the NSGA-II method under the same edge-cloud architecture. In essence, the novelty of this study does not lie in the application of each of MPC, digital twin, and anomaly detection individually but rather in their integration via a reliable-state mechanism. The significant research contributions of this paper can be stated as follows:

- An IoT-based edge-cloud system architecture has been devised to off-load time-sensitive control tasks to the edge and compute-intensive tasks of training and optimization to the cloud.
- Channel-wise reliability weighted data fusion method has been adopted for continuous fusion of physical sensor readings and digital-twin based readings before running MPC.
- Reliability-gated adaptive digital twin is used for offering alternate state estimates and minimizing impact of any corrupted sensor readings on model updates.
- BO, PSO, and NSGA-II have been utilized for prediction, tuning of anomaly detector, and multi-objective MPC parameter selection, respectively.
- Performance of the proposed framework is analyzed against four baseline controllers in terms of control, economics, detection, and edge processing performance in nominal, cloud-load, FDI, and hybrid cyber-physical scenarios.

2. LITERATURE SURVEY

Recent research on intelligent microgrids has focused on digital-twin modeling, predictive energy management, distributed control, data-driven forecasting, and cyberattack detection. Digital twins improve the interaction between physical energy systems and their virtual representations, while model predictive control and optimization algorithms coordinate distributed energy resources under operational constraints. In parallel, machine-learning methods have been employed to process high-dimensional measurements and identify false-data injection attacks. However, these areas are commonly investigated as separate functions, with limited integration among measurement reliability, digital-twin state estimation, big-data analytics, optimization, and resilient closed-loop control.

O'Dwyer *et al*. developed an energy-management and digital-twin platform for coordinating multi-vector smart-energy systems in 2020 [15]. Their method combined machine-learning forecasting, model predictive control, and a modular optimization architecture to coordinate communal heating and electric-vehicle charging systems. The digital-twin environment was used to test control decisions before their application to the physical assets. The case studies demonstrated that different energy subsystems could be coordinated while avoiding violations of high-level operational constraints. However, the framework was designed for district-level energy coordination and did not investigate photovoltaic–battery voltage regulation, cyberattacks, measurement uncertainty, or reliability-based sensor fusion.

Following that, the authors Gupta *et al*. proposed a grid-aware distributed MPC framework for heterogeneous energy resources [16]. Their approach consisted of day-ahead scheduling followed by real-time distributed predictive control, in which active and reactive power references were determined while respecting nodal-voltage, line-ampacity, and device-level constraints. Experimental validation on a real-scale microgrid based on the CIGRE benchmark confirmed that the method could track an aggregated dispatch plan while maintaining grid constraints. Nevertheless, the controller relied on trustworthy measurements and an accurate network model, and it did not consider digital-twin estimation, communication anomalies, or false-data injection attacks.

Semeraro *et al*. presented a systematic analysis of the digital-twin paradigm in 2021 [17]. The authors reviewed digital-twin definitions, architectures, lifecycle applications, enabling technologies, and information-exchange mechanisms. Their study established a structured distinction among digital models, digital shadows,

and fully synchronized digital twins and identified IoT connectivity, simulation, artificial intelligence, and bidirectional data exchange as major enabling technologies. Although the study provided an important theoretical foundation, it remained application-independent and did not formulate or validate a digital-twin controller for renewable-energy microgrids. It also did not address how unreliable measurements should be incorporated into the virtual model.

Li *et al*. introduced a secure federated deep-learning method for detecting false-data injection attacks in smart grids in 2022 [18]. Transformers were used as detectors at the edge node level to learn the associations between electrical signals, whereas federated learning was utilized for collaborative training of the model without sending local data to the central server. The model update process was further secured using the Paillier cryptosystem. Experimentation on the IEEE 14-bus and 118-bus systems showed better results than the considered local and centralized learning approaches in detecting attacks. Nonetheless, the paper concentrated on the identification of attacks and privacy protection but did not relate detection certainty to predictive control or digital twins.

In 2023, Othman *et al*. explored digital twinning for smart grid communication networks [19]. In this paper, digital twinning was explained as providing real-time monitoring, proactive allocation of radio resources, communication, and service recovery after unexpected events in the network. Digital twinning as a method of coordination between the physical grid and communication/computational resources was highlighted in the research. The challenges of implementation were identified as real-time synchronization, model abstraction, interoperability, computational challenges, and cybersecurity. However, the research was largely architectural and communication-related, and no photovoltaic-battery controller in a closed loop or voltage regulation analysis was presented.

Qi *et al*. developed a prediction-free coordinated optimization framework for a microgrid containing hybrid hydrogen and battery storage in 2025 [20]. Their method used a semi-empirical hydrogen-storage model, historical optimal state-of-charge trajectories, kernel-regression-based reference updating, and adaptive virtual-queue online convex optimization. Numerical studies using the Elia and North China datasets showed reductions of approximately 30% in operating cost and 80% in loss of load compared with existing online optimization approaches. Despite these improvements, the study addressed long-term hydrogen–battery scheduling rather than fast photovoltaic–battery voltage control. It also did not consider digital-twin synchronization, cyberattacks, corrupted measurements, or anomaly-aware control.

Huang *et al*. proposed a data-driven, prediction-free real-time dispatch approach for microgrids with generalized energy storage in 2025 [21]. Offline optimization was first used to obtain representative state-of-charge trajectories, after which kernel, regression generated dynamic references and opportunity prices. An adaptive virtual-queue algorithm based on online convex optimization then determined the real-time dispatch. Compared with MPC-based strategies, the method reduced operating cost by approximately 5% and voltage-violation rate by approximately 9%. However, the reported validation was simulation-based and concentrated on economic dispatch under uncertain forecasts. The effects of sensor corruption, packet loss, digital-twin model mismatch, and reliability-weighted state estimation were not examined.

More recently, Doumèche *et al*. investigated large-scale electricity-demand forecasting during the French energy crisis in a 2026 journal paper [22]. In addition to traditional weather and calendar features, the researchers used mobility-related information obtained through mobile network data to reflect drastic shifts in human behavior. It was found that using such information on spatial mobility improved forecasting outcomes compared to state-of-the-art methods during the unusual energy-saving period. Such an approach proves that heterogeneous sources of big data can be valuable when traditional trends do not hold. However, the method has been designed specifically for national-level power consumption forecasting and does not consider other components of the system.

A structured comparative synthesis of the selected papers in relation to their methodologies, findings, and limitations is presented in Table 1. There has been a considerable amount of progress made in the areas of digital twin modeling, distributed predictive control, forecasting, attack detection, and energy management. However, it also reveals that these functions are generally addressed in isolation, with limited consideration of their coordinated influence on closed-loop microgrid performance. In particular, the reviewed studies rarely integrate measurement reliability, digital-twin state reconstruction, big-data analytics, and multi-objective control within a unified photovoltaic–battery microgrid framework.

Thus, the uniqueness of this approach lies in the integration of the measurement trust evaluation and control prediction processes. The existing cyber-resilient methods usually place attention on the attack detection, secure communication, resilient control, and measurement substitution independently. However, in this approach, the anomaly information of each channel is transformed into the reliability coefficient that determines the contribution of physical measurement and its digital-twin estimation to the state that will be

provided to the MPC. Thus, it creates the gradient reaction to uncertain measurements instead of accept/reject method.

Table 1. Summary of the Reviewed Literature

Ref.	Authors, Year	Method and Contribution	Main Results	Limitations
[15]	O'Dwyer *et al.*, 2020	Digital-twin energy-management platform integrating forecasting, MPC, and multi-energy optimization.	Coordinated heating and electric-vehicle charging while satisfying system constraints.	Did not consider microgrid voltage regulation, cyberattacks, or measurement reliability.
[16]	Gupta *et al.*, 2020	Distributed MPC for scheduling and real-time control of heterogeneous energy resources.	Experimentally tracked dispatch targets while maintaining voltage, line, and device constraints.	Assumed reliable measurements and an accurate network model.
[17]	Semeraro *et al.*, 2021	Systematic review of digital-twin architectures, enabling technologies, and data exchange.	Established classifications and fundamental requirements for synchronized digital twins.	No microgrid controller or quantitative experimental validation.
[18]	Li *et al.*, 2022	Transformer-based secure federated learning with Paillier encryption for FDIA detection.	Improved attack detection on IEEE 14- and 118-bus systems while preserving data privacy.	Detection results were not integrated into closed-loop control or measurement recovery.
[19]	Othman *et al.*, 2023	Digital-twin architecture for monitoring and communication-resource management in smart grids.	Demonstrated potential for proactive resource allocation and service restoration.	Mainly conceptual and communication-oriented, without physical microgrid control validation.
[20]	Qi *et al.*, 2025	Prediction-free online optimization for hybrid hydrogen–battery microgrid management.	Reduced operating cost by approximately 30% and loss of load by approximately 80%.	Focused on long-term scheduling rather than cyber-resilient voltage control.
[21]	Huang *et al.*, 2025	Data-driven online convex optimization using dynamic SOC references and virtual queues.	Reduced operating cost by about 5% and voltage violations by about 9%.	Did not consider corrupted measurements, anomaly detection, or digital-twin fusion.
[22]	Doumèche *et al.*, 2026	Electricity-demand forecasting using meteorological, calendar, and mobile-network mobility data.	Mobility features improved forecasting during abnormal energy-consumption conditions.	National-level forecasting study without microgrid control, battery modeling, or cybersecurity analysis.

3. PROPOSED METHODOLOGY

The proposed framework is organized into four essential phases, as illustrated in Figure 2. These phases integrate physical microgrid modelling, big-data processing, forecasting, adaptive digital-twin estimation, anomaly-aware measurement fusion, and optimization-assisted predictive control within a unified closed-loop structure. The output of each phase is transferred to the next phase, while the final control commands are applied to the physical photovoltaic–battery microgrid.

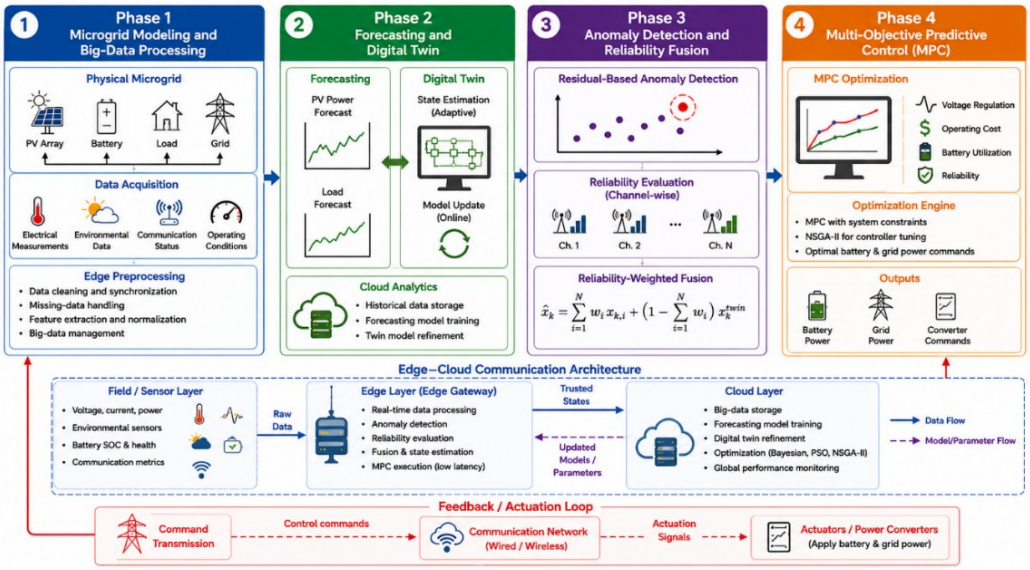


Figure 2. Proposed methodology phases

3.1. Phase 1: Microgrid Modeling and Big-Data Processing

The first phase establishes the physical photovoltaic–battery microgrid and prepares the heterogeneous data required by the intelligent control framework. The system consists of a photovoltaic source, battery energy-storage system, DC bus, local load, and grid interface. The instantaneous power balance is expressed as shown in Equation (1) [23]:

$$P_{PV}(t) + P_{bat}(t) + P_{grid}(t) - P_{load}(t) = P_{loss}(t), \tag{1}$$

where P_{PV}, P_{bat}, P_{grid}, and P_{load} denote the photovoltaic, battery, grid, and load powers, respectively, while the P_{loss} represents converter and system losses.

The DC-bus dynamics are modeled by utilizing the following mathematical expression which presented in Equation (2):

$$C_{dc}\frac{dV_{dc}(t)}{dt} = \frac{P_{PV}(t) + P_{bat}(t) + P_{grid}(t) - P_{load}(t)}{V_{dc}(t)}, \tag{2}$$

where C_{dc} is the DC-link capacitance and V_{dc} is the bus voltage. The battery state of charge is updated according to the following mathematical expression as describes in Equation (3) [24]:

$$SOC(k+1) = SOC(k) - \frac{\eta_{bat}P_{bat}(k)\Delta t}{E_{bat}}, \tag{3}$$

where E_{bat} is the battery capacity, η_{bat} is the charging or discharging efficiency, and Δt is the sampling interval.

The data layer collects electrical, environmental, battery, and communication variables can be presented as shown in Equation (4) [24]-[26]:

$$\mathrm{z}(k) = [P_{PV}, P_{load}, V_{dc}, SOC, G, T, \tau_{net}, L_{pkt}], \tag{4}$$

where G is solar irradiance, T is referring to the temperature, τ_{net} is communication latency, and L_{pkt} represents packet-loss status. The acquired measurements are synchronized, filtered, normalized, and divided into training, validation, and testing datasets.

In order to prevent any information leakage, the three subsets are separated during the whole process of model training, parameter adjustment and performance estimation. The training subset is employed to train forecasting models, whereas the validation subset is used by the Bayesian optimization procedure to estimate the forecasting history and the hyperparameters of forecasting models. The last one, test subset, is not utilized for any of these steps and is reserved only for estimating the final performance of forecasting and closed-loop control procedures. The same applies to the tuning of the anomaly detector parameters by PSO. For this, the calibration dataset with normal residual pattern and artificial attack cases is utilized, whereas the testing dataset is not used in the PSO search process.

Edge processing is used for low-latency filtering, residual generation, and anomaly evaluation, whereas the cloud layer is used for historical storage, forecasting-model training, and optimization. Cyclic time features are also extracted to represent daily renewable and load patterns as presents in both Equation (5) and Equation (6) [27]-[29]:

$$f_{sin}(k) = \sin\left(\frac{2\pi h(k)}{24}\right), \tag{5}$$

$$f_{cos}(k) = \cos\left(\frac{2\pi h(k)}{24}\right), \tag{6}$$

where $h(k)$ is referring to the hour of the day.

3.1.1. Networked Edge–Cloud Communication Architecture

The control system is implemented within an edge–cloud framework that brings together the photovoltaic generation unit, battery energy storage system, loads, digital twin, power converters, and supervisory predictive controller. Distributed sensors collect electrical, environmental, battery, and communication-related information, including DC-bus voltage, photovoltaic power, load power, battery state of charge, packet loss, and communication delay. These measurements are then transmitted to the edge gateway through the microgrid communication system [30].

The communication architecture is organized into three main layers: the field/device layer, the edge-control layer, and the cloud layer. The field layer contains the distributed electrical, environmental, battery, and communication-status sensors, together with the converter actuators. The collected measurements are forwarded to the edge gateway, where time-sensitive tasks such as data synchronization, filtering, residual calculation, anomaly detection, channel-wise reliability assessment, trusted-state construction, and MPC execution are performed locally. More computationally intensive and less time-critical operations are handled by the layer of the cloud. These include historical data storage, forecasting-model training, digital-twin refinement, Bayesian optimization, PSO-based detector tuning, and NSGA-II-based controller optimization. Updated models and optimized parameters are then sent from the cloud to the edge controller, while the resulting control commands are transmitted from the edge gateway to the converter actuators.

In this study, the communication module is modelled at the functional level and does not correspond to any particular wired or wireless communication protocol, nor does it relate to a particular edge-computing infrastructure. Communication delays and packet-loss instances are treated as network status variables and disturbances rather than being simulated by means of a protocol-level network simulator. Similarly, the mentioned edge-processing delay corresponds to the computation time of the local algorithmic computations and cannot be treated as a benchmark of any particular processor or gateway, as well as its software environment. As a consequence, communication protocol-related aspects such as access latency, routing overhead, retransmission policies, bandwidth conflicts, communication jitter, and wireless node energy expenditure are not taken into account within the scope of this simulation and have to be validated separately.

The bidirectional communication links carry sensor measurements from the physical microgrid to the edge controller and control commands from the controller to the converter actuators. Communication and cyber disturbances, including packet loss, delay, replay attacks, and false-data injection, may reduce the reliability of the received measurements. To reduce their influence on the control process, the proposed framework combines physical residuals, digital-twin estimates, and channel-wise reliability information to construct a trusted-state vector before the measurements are used by the MPC [31].

3.2. Phase 2: Forecasting and Adaptive Digital-Twin Development

The second phase combines data-driven forecasting with an adaptive digital twin. The forecasting model uses historical windows of photovoltaic, load, environmental, and time-dependent variables to estimate future renewable generation and demand over the prediction horizon as shown in both Equation (7) and Equation (8) [32]-[35]:

$$\hat{P}_{PV}(k+1:k+N_p), \tag{7}$$

$$\hat{P}_{load}(k+1:k+N_p), \tag{8}$$

where N_p denotes the prediction horizon.

Forecasting performance is evaluated by utilizing RMSE, MAE, MAPE, and R^2. The RMSE is calculated as depicts in Equation (9) [33]-[35]:

$$RMSE = \sqrt{\frac{1}{N}\sum_{k=1}^{N}[y(k)-\hat{y}(k)]^2}. \tag{9}$$

Bayesian optimization is employed to tune the forecasting-model parameters because every candidate evaluation requires model training and validation. The optimal forecasting parameters are obtained from the following expression as describes in both Equation (10) and Equation (11):

$$\Theta_F^* = \arg\min_{\Theta_F} J_F(\Theta_F), \tag{10}$$

$$J_F = \frac{1}{2}\frac{RMSE_{PV}}{\bar{P}_{PV}} + \frac{1}{2}\frac{RMSE_{load}}{\bar{P}_{load}}. \tag{11}$$

The resulting forecasts are supplied directly to the predictive controller. In parallel, the digital twin reproduces the principal dynamics of the physical microgrid. Its state-space representation is given by the following expression as presents in both Equation (12) and Equation (13):

$$\hat{x}(k+1) = \hat{A}(k)\hat{x}(k) + \hat{B}(k)u(k) + \hat{E}(k)d(k), \tag{12}$$

$$\hat{\mathrm{x}}(k) = [\hat{V}_{dc}(k), \widehat{SOC}(k)]^T, \tag{13}$$

where $\mathrm{u}(k)$ contains the battery and grid control actions, and $\mathrm{d}(k)$ includes the photovoltaic and load disturbances [36][37].

The parameters of the digital twin are updated online through recursive least squares algorithm. In order to avoid the pollution of the model through erroneous data, the updating process takes place only if the incoming data fulfills the pre-set reliability criteria. The adaptation process is causal in nature, meaning that at each sampling instant, the digital twin makes use of only the available data till then and not the future data samples or test results. This ensures that the data from the subsequent tests does not affect the updating of the model at the current instant.

3.3. Phase 3: Anomaly Detection and Reliability-Weighted Data Fusion

The third phase of the proposed work evaluates the reliability of the measured signals and constructs the trusted state vector used by the controller. The anomaly detector compares each physical measurement with the corresponding digital-twin estimate. The normalized residual of the i-th measurement is expressed as shown in Equation (14) [38]:

$$e_i(k) = \frac{| y_i(k) - \hat{y}_i^{DT}(k) |}{\sigma_i + \varepsilon}, \tag{14}$$

where σ_i denotes the residual scale and ε is a small constant used to avoid numerical singularities.

The residual is smoothed using an exponentially weighted moving average is represented as depicts in Equation (15):

$$s_i(k) = \lambda_A s_i(k-1) + (1-\lambda_A) e_i(k), \tag{15}$$

where λ_A is the smoothing coefficient. The measurement reliability is subsequently determined as describes in Equation (16):

$$r_i(k) = \exp\left[-g\max\left(0, s_i(k) - \gamma\right)\right], \tag{16}$$

where γ is the anomaly threshold and g controls the reliability-decay rate.

Particle swarm optimization is employed to tune the anomaly-detection parameter vector, and the corresponding PSO objective function is defined as determined by both Equation (17) and Equation (18) according to [39]-[40]:

$$\Theta_A = [\gamma, \lambda_A, g]. \tag{17}$$

$$\Theta_A^* = \arg\min_{\Theta_A} [1 - F_1 + \alpha FAR], \tag{18}$$

where F_1 is the detection F1-score, FAR is the false-alarm rate, and α is a weighting coefficient. This objective encourages high attack-detection capability while penalizing false alarms during normal microgrid variations.

Instead of applying complete binary replacement, the proposed framework performs continuous reliability-weighted fusion as given in Equation (19):

$$\tilde{y}_i(k) = r_i(k) y_i(k) + [1 - r_i(k)] \hat{y}_i^{DT}(k). \tag{19}$$

When $r_i(k)$ approaches one, the physical measurement receives the dominant weight. When the reliability decreases, the controller gradually depends more strongly on the digital-twin estimate. The trusted state vector is expressed as presents in Equation (20):

$$\tilde{\mathrm{x}}(k) = [\tilde{V}_{dc}(k), \widetilde{SOC}(k), \tilde{P}_{PV}(k), \tilde{P}_{load}(k)]^T. \tag{20}$$

This constant blending avoids abrupt switches and prevents the impact of faulty data points without relying completely on the simulated model.

3.4. Phase 4: Multi-Objective Predictive Control and Performance Evaluation

In this final step, the battery and grid powers are calculated via model predictive control, which takes as input the reliable states, photovoltaic and load forecast data, battery capacity, and grid limitations. Its objective function is formulated as depicts in Equation (21) [41]:

$$J_{MPC} = \sum_{j=1}^{N_p} [\Big[\quad w_V \left(V_{dc}(k+j) - V_{dc}^{ref}\right)^2 + \quad w_{SOC}(SOC(k+j) - SOC^{ref})^2 + \quad w_{bat} P_{bat}^2(k+j) + w_{grid} P_{grid}^2(k+j) + \quad w_{\Delta u} \parallel \Delta \mathrm{u}(k+j) \parallel_2^2]. \tag{21}$$

The optimization is performed subject to the main physical and operational constraints of the microgrid, ensuring safe and stable system operation. Accordingly, the DC-bus voltage, battery state of charge, battery power, and grid power are maintained within their predefined limits as determined by Equation (22):

$$\begin{aligned} V_{dc}^{min} \le V_{dc}(k) \le V_{dc}^{max}, \\ SOC_{min} \le SOC(k) \le SOC_{max}, \\ P_{bat}^{min} \le P_{bat}(k) \le P_{bat}^{max}, \\ P_{grid}^{min} \le P_{grid}(k) \le P_{grid}^{max}. \end{aligned} \tag{22}$$

The controller-weight vector contains the main weighting coefficients used to balance voltage regulation, battery state-of-charge tracking, battery utilization, grid-power exchange, and control-action variation. It is defined as given by Equation (23):

$$\Theta_C = [w_V, w_{SOC}, w_{bat}, w_{grid}, w_{\Delta u}]. \tag{23}$$

NSGA-II is employed to optimize these weights because the controller must balance several conflicting objectives as describes in Equation (24) [42][43]:

$$\begin{aligned} f_1 = RMSE_{V_{dc}}, \\ f_2 = C_{energy} + C_{battery}, \\ f_3 = E_{battery}, \end{aligned} \tag{24}$$

where C_{energy} is the grid-energy cost, $C_{battery}$ is referring to the battery-utilization cost, and $E_{battery}$ represents battery throughput. This algorithm generates a Pareto-optimal set of solutions, and the final set of parameters is chosen through the use of a normalized knee point criteria for achieving an acceptable compromise between the objectives.

Optimization through NSGA-II is done in the offline design phase of the controller with test cases which are separated from the actual evaluation process. The Pareto-optimal control weights are chosen based on the knee point criterion prior to the actual testing of the test cases. After the selection, the MPC weight vector is not tuned any further according to the test results. This separation helps ensure that the final evaluation scenarios do not directly influence controller-parameter selection and reduces the risk of information leakage.

4. RESULTS AND DISCUSSION

The proposed framework was evaluated under nominal operation, rapid photovoltaic and load variations, FDI, and mixed cyber-physical anomalies. Five control strategies were examined: rule-based control, conventional MPC, forecast-assisted MPC, digital-twin MPC with binary measurement replacement (DT-MPC), and the proposed reliability-weighted digital-twin MPC. The evaluation looked into forecasting accuracy, voltage regulation, cost of operation, battery usage, anomaly detection effectiveness, computational delay, and controller viability.

4.1. Optimization and Forecasting Performance

Figure 3 presents the convergence behavior of particle swarm optimization during anomaly-detector tuning. The best objective value decreased from 0.1197 in the first iteration to 0.0894 by the fifth iteration, corresponding to a reduction of approximately 25.33%. The optimized detector parameters were a residual threshold of 2.7654, a smoothing coefficient of 0.5, and a reliability-decay gain of 0.2. The solution remained unchanged during the remaining iterations, indicating early convergence of the detector-tuning process.

For setting the forecasting window and regularization, Bayesian optimization has been used. In the tested setups, the best objective value is achieved by choosing a forecasting window length of 26 samples and a regularization value of 0.9987. All other setups have the objective value ranging from 0.07263 to 0.07501.

Table 2 summarizes the forecasting results. Load forecasting achieved an RMSE of 2.327 kW, MAPE of 8.06%, and $R^2$of 0.306. In contrast, the photovoltaic model produced an RMSE of 0.668 kW and a negative $R^2$of -0.384, indicating that the present forecasting configuration did not adequately represent rapid photovoltaic variations.

The forecasting results highlight an important limitation of the proposed framework. Although the load model was able to capture the general demand pattern, the PV forecasting model showed limited accuracy during rapid irradiance variations, with an RMSE of 0.668 kW, a MAPE of 46.68%, and a negative R^2 value of -0.384. Thus, the enhanced performance of the closed loop with the use of the developed framework should not be directly associated with high forecasting accuracy of the PV data. Within the proposed control scheme, the PV and load forecasts serve as an auxiliary element that gives additional data over the prediction horizon, whereas the controller is updated at each step with the help of the reliable states determined through channel-wise reliability analysis and digital twins' fusion. Therefore, the primary source of anomalies robustness is the reliable state estimation technique instead of the forecasting block itself. Poor forecasting performance is also in line with worse performance of the proposed controller during rapid changes in cloud-load conditions, when conventional MPC yielded better results in terms of voltage RMSE.

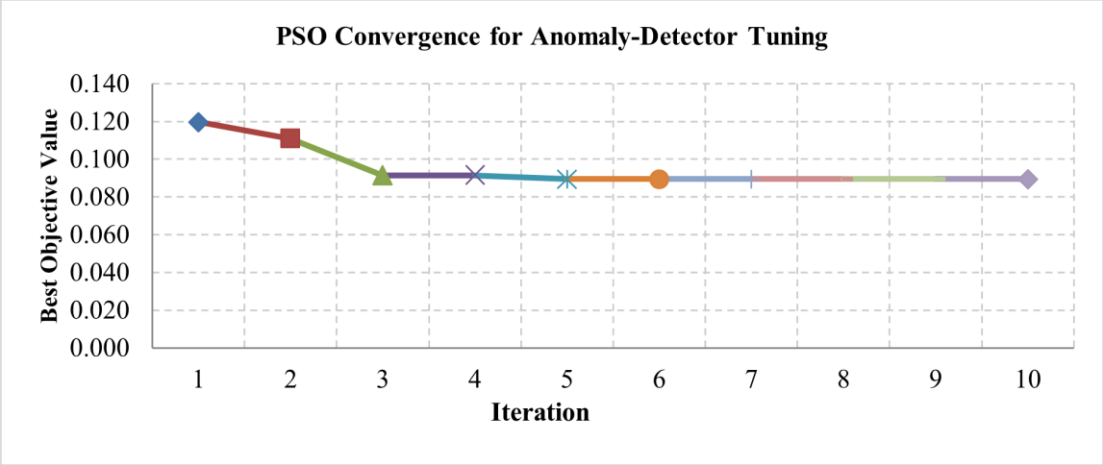


Figure 3. PSO convergence for anomaly-detector tuning

Table 2. Forecasting performance

Signal	RMSE (kW)	MAE (kW)	MAPE (%)	R^2
PV power	0.668	0.520	46.68	−0.384
Load demand	2.327	1.822	8.06	0.306

4.2. Aggregate Control Performance

Figure 4 and Table 3 summarize the aggregate voltage-regulation and operating-cost performance across the four investigated scenarios. As shown in the left panel of Figure 4, the proposed method achieved the lowest mean voltage RMSE of 1.561 V, compared with 2.016 V for the rule-based controller, 2.159 V for conventional MPC, 2.331 V for Forecast-MPC, and 3.204 V for DT-MPC. These values correspond to RMSE reductions of 22.57%, 27.69%, 33.01%, and 51.28%, respectively. However, this aggregate advantage should not be interpreted as uniform superiority under all operating conditions, since conventional MPC achieved lower voltage RMSE under both nominal and cloud–load conditions, as discussed in Section 4.3. In terms of operating cost, Forecast-MPC achieved the lowest mean value of 23.801, followed by DT-MPC at 26.601, conventional MPC at 26.699, the proposed method at 28.814, and rule-based control at 31.601. The proposed framework therefore required approximately 21.06% higher operating cost than Forecast-MPC, indicating a trade-off between economic performance and anomaly-resilient voltage regulation. Nevertheless, the proposed method reduced the operating cost by approximately 8.82% compared with the rule-based strategy.

Although the proposed method provided the best overall voltage regulation, it did not achieve the lowest operating cost. Forecast-MPC produced the lowest mean cost of 23.801, whereas the proposed framework obtained 28.814, which was approximately 21.06% higher. This difference indicates that the proposed controller used additional grid and battery actions to maintain resilience under corrupted measurements. However, its battery throughput remained substantially lower than the 133.976 kWh produced by Forecast-MPC, showing that the resilience improvement was not achieved through unrestricted battery cycling.

The mean value of 95th percentile latency of the developed approach is 2.422 ms, and the MPC solver success rate still equals to about 99.86% for all analyzed cases. This means that the additional step of reliability assessment and digital twin fusion was computationally cheap.

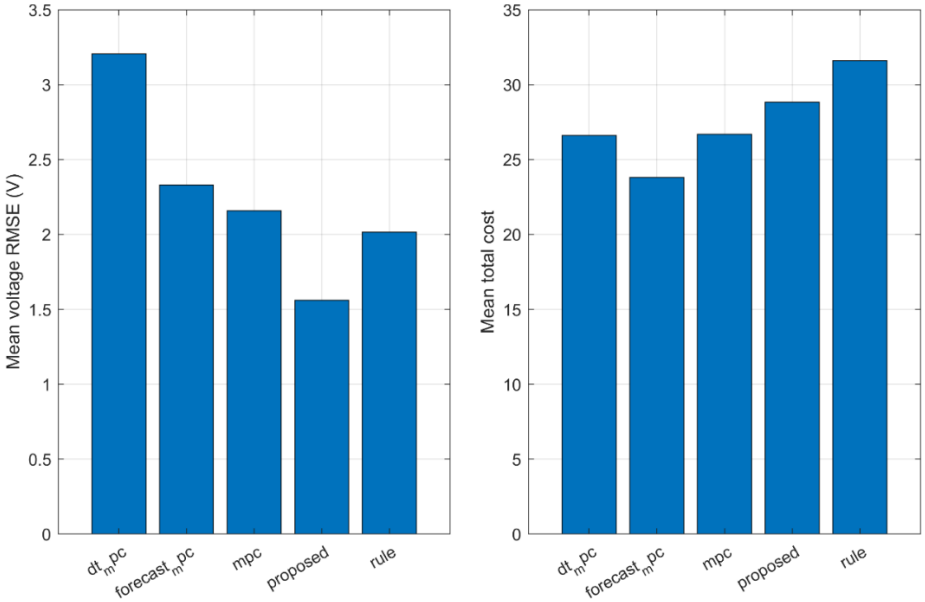


Figure 4. Aggregate voltage-regulation and operating-cost comparison

Table 3. Aggregate performance of the evaluated control methods

Method	Voltage RMSE, mean ± SD (V)	Mean total cost	Battery throughput (kWh)	Mean detector F1	P95 latency (ms)
Rule-based	2.016 ± 1.777	31.601	66.384	0.273	0
MPC	2.159 ± 2.278	26.699	95.313	0.269	2.673
Forecast-MPC	2.331 ± 2.090	23.801	133.976	0.308	2.369
DT-MPC	3.204 ± 1.856	26.601	80.939	0.296	2.517
Proposed	1.561 ± 1.115	28.814	88.458	0.312	2.422

4.3. Scenario-Wise Performance

The comparative performance of the tested control algorithms with respect to the four different operational conditions is presented in Table 4. Differences between normal operation, rapid physical changes, and attacks are emphasized. In nominal operation and cloud-load conditions, the F1-score is specified as not applicable since no attacks take place in these conditions and thus there are no positive anomaly examples available for performance analysis. As a result, an F1-value equal to zero in such cases cannot be considered a failure of the anomaly detection algorithm. Voltage regulation performance and operating cost are the major performance indices in such cases, while the F1-score is important only when there are abnormal data in the FDI and mixed-anomaly cases.

When the system operates nominally, the conventional MPC obtains the lowest RMSE of 0.296 V in voltage, as opposed to 0.391 V obtained by the proposed control system. The implication here is that the reliability evaluation and digital twin integration algorithms do not offer much advantage when there is no cyber-physical attack on the measurement and the measurement is still reliable.

Under the cloud-load disturbance, MPC performed once again with the minimum voltage RMSE of 0.287 V compared to that of the proposed control at 2.338 V. The poor performance of the proposed method in response to rapid physical disturbances suggests that any abrupt change in PV and loads might make physical disturbance behave like measurement anomaly, thus decreasing the confidence on valid transient measurement. In conclusion, it is clear that the proposed method's strength comes from handling measurement anomalies and not physical disturbances.

This degradation is compatible with the lower PV forecasting precision mentioned in Section 4.1. In fast-changing irradiation conditions, inaccuracies of the forecasted PV curve can negatively impact the quality of the horizon information provided to the predictor. That is why the new approach is not designed to be better

than classical MPC for all cloud-load interferences based only on physical processes. The real value of the new approach is revealed when data reliability deteriorates due to false data injection and cyber-physical attacks.

The most significant improvement was observed under FDI. The proposed method reduced voltage RMSE to 0.843 V, compared with 4.926 V for MPC, 4.934 V for Forecast-MPC, and 1.435 V for DT-MPC. These values correspond to reductions of 82.89%, 82.92%, and 41.28%, respectively. The detector F1-score also increased to 0.564, which was the highest value among the evaluated methods.

Under mixed anomalies, the proposed controller achieved the lowest voltage RMSE of 2.674 V. This represented improvements of 14.56% relative to MPC, 13.96% relative to Forecast-MPC, 26.64% relative to rule-based control, and 43.39% relative to DT-MPC. Its F1-score of 0.684 was approximately equal to the highest result produced by Forecast-MPC. The complete scenario results, including voltage deviation, cost, battery throughput, renewable utilization, and detection indices, are provided in the simulation output.

Table 4. Scenario-wise voltage, cost, and detection performance

Method	Nominal RMSE / cost	Cloud–load RMSE / cost	FDI RMSE / F1	Mixed RMSE / F1
Rule-based	0.486 / 30.569	0.472 / 34.501	3.463 / 0.468	3.644 / 0.623
MPC	0.296 / 27.208	0.287 / 31.139	4.926 / 0.453	3.129 / 0.621
Forecast-MPC	0.553 / 21.344	0.728 / 25.552	4.934 / 0.546	3.107 / 0.684
DT-MPC	1.770 / 26.737	4.890 / 26.489	1.435 / 0.537	4.722 / 0.648
Proposed	0.391 / 27.350	2.338 / 30.571	0.843 / 0.564	2.674 / 0.684

4.4. Time-Domain Response under Mixed Anomalies

Figure 5 depicts the time-domain responses of the DC-bus voltage and the battery SoC for all five control methods, along with the anomaly score and its corresponding threshold value in the mixed cyber-physical anomaly case. From the voltage profiles, the proposed approach was successful in limiting the deviation compared to the rule-based, conventional MPC, Forecast-MPC, and DT-MPC approaches during the primary anomaly periods. In addition, the voltage profile of the proposed approach converged faster toward the 750 V reference value compared to the DT-MPC, where the voltage level stayed much lower than the reference from around 6.5 to 8 h.

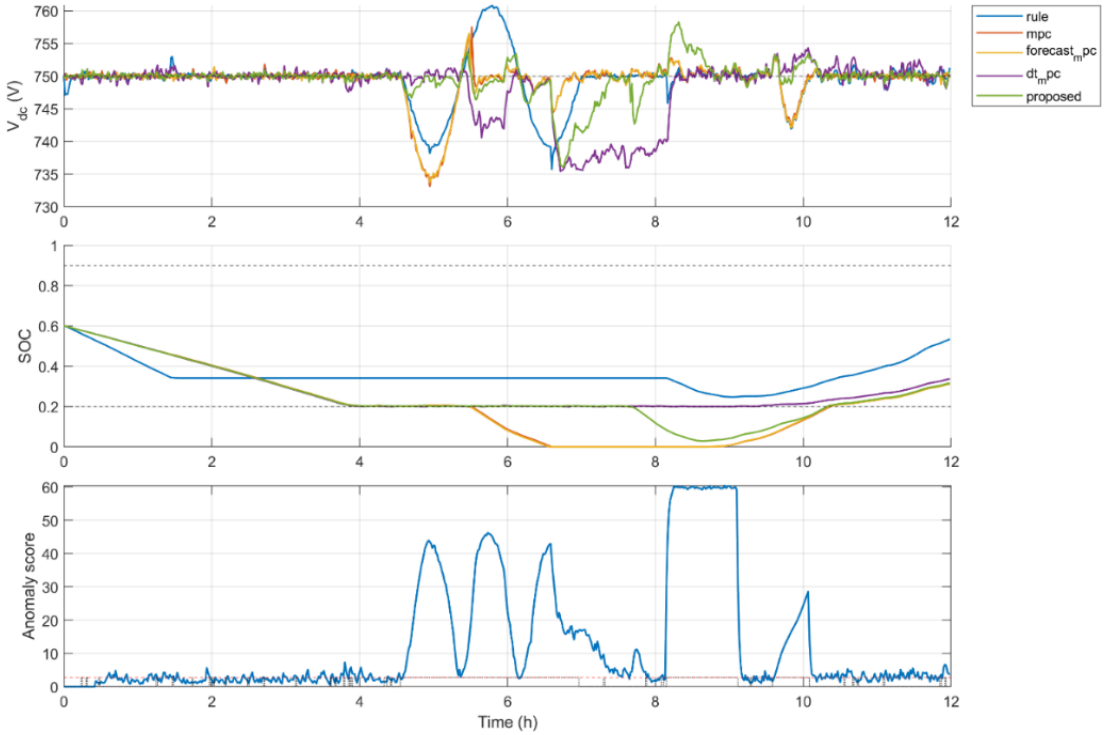


Figure 5. Comparative DC-bus voltage, battery SOC, and anomaly-score responses under mixed cyber-physical anomalies

The results obtained regarding SOC responses indicate the existence of a compromise that is necessary to be considered when designing the control algorithm. Rule-Based Control kept the battery inside the working

interval; however, this approach exhibited poorer voltage regulation capabilities. On the other hand, the use of MPC and Forecast-MPC led to violation of the lower boundary of the SOC for a prolonged period. The suggested approach resulted in an SOC violation ratio of 22.5%, while for MPC and Forecast-MPC, it was 40.69% and 40.56%, respectively. Thus, the suggested system ensured better battery safety than the other predictive control methods while ensuring voltage regulation robustness.

There is a significant rise in the anomaly score when there are cyber-physical disturbances being injected and there is a fall in the score after the disturbances have been taken away from the system. The above pattern indicates that the anomaly detector can detect anomalies in the system but there is partial sensitivity even in normal operation conditions of the system.

4.5. Reliability-Weighted Fusion and Anomaly Detection

Figure 6 shows the functioning of the proposed reliability-weighted fusion scheme in case of mixed cyber-physical attacks. The upper plot provides the comparison of the distorted voltage measurements, the trustworthy voltage used for the controller and the actual one, while the lower plot shows the time-varying reliability of voltage, SOC, PV power and load channels. During the main attacks the measured voltage varied within the range of about 727 and 772 V, while the trustworthy signal was much closer to the nominal value of 750 V. This example shows that the proposed reliability-based fusion scheme successfully suppresses the impact of the distorted measurements, which becomes progressively smaller as the corresponding reliability drops, making the digital twin estimation more reliable. Thus, the channel-wise reliability behaviour shows that the proposed approach allows detecting the trustworthiness of the data at runtime, which gives an opportunity to provide a more reliable state estimation for the predictive controller. The anomaly-detection performance under the FDI and mixed anomalies is shown in Table 5.

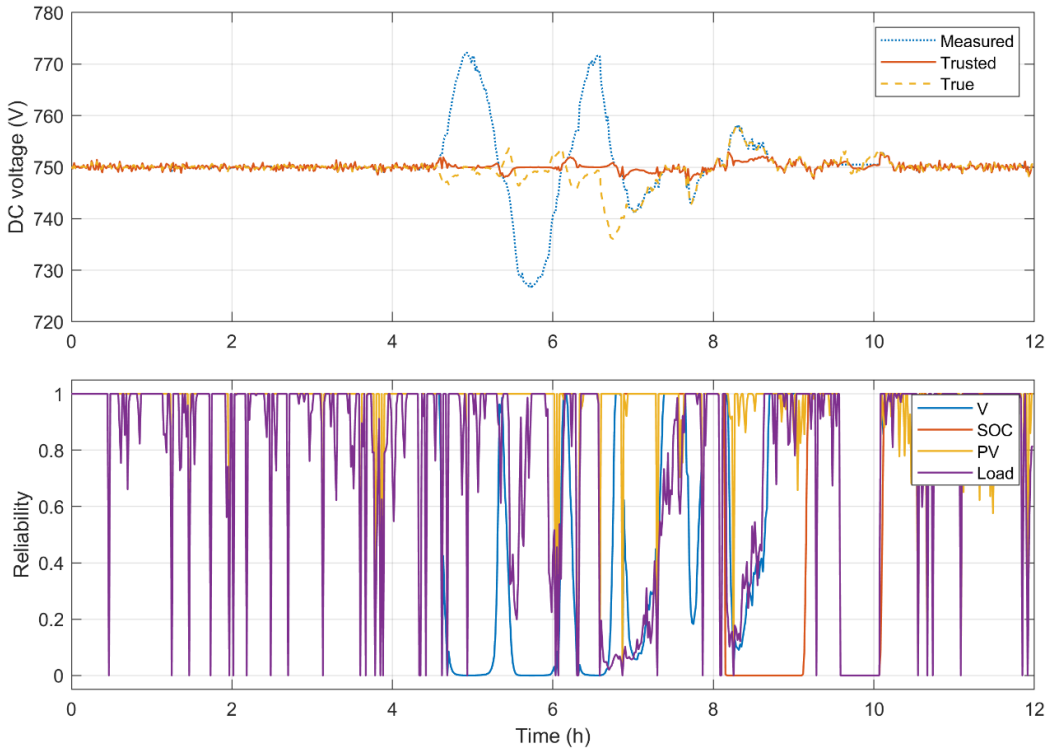


Figure 6. Reliability-weighted fusion of measured and digital-twin voltage signals with channel-wise reliability scores

Table 5. Anomaly-detection performance

Scenario	Method	Precision	Recall	F1-score	False-alarm rate
FDI	Forecast-MPC	0.387	0.924	0.546	0.369
FDI	DT-MPC	0.367	1.000	0.537	0.435
FDI	Proposed	0.399	0.959	0.564	0.363
Mixed	Forecast-MPC	0.557	0.886	0.684	0.408
Mixed	DT-MPC	0.503	0.909	0.648	0.520
Mixed	Proposed	0.548	0.909	0.684	0.434

The suggested anomaly detector retained its high sensitivity in both attack situations, with recall scores of 0.959 and 0.909 in the FDI and mixed cases, respectively. Nevertheless, the false alarm ratios were still quite high, at 0.363 and 0.434, respectively, and this can be regarded as a drawback of the proposed approach. It shows that some system variations that are considered normal can be classified as abnormal ones. The same pattern can be seen in the reliability reactions for individual channels, in particular for the load and SOC channels, which exhibited temporary dips in their reliability levels during normal system transients. Sudden shifts in PV power generation, load demand, and battery operation can cause traces that are very similar to those produced by faulty data, thus making it harder for the anomaly detector to differentiate them from each other. Consequently, the existing system detector becomes more sensitive to anomalies in general than selective to filtering out false positives. Even though it does not affect the detection recall, the increased frequency of false positives could decrease the confidence in the results of measurement, use the values estimated by a digital twin more often, and adopt more cautious control. In real-world settings, they can additionally increase the monitoring workload and undermine confidence in the detection process. Thus, further optimization is required to minimize the number of false positives while not decreasing the sensitivity of the detector to abnormalities.

4.6. Multi-Objective Optimization Analysis

The Pareto front obtained by applying the NSGA-II method is shown in Figure 7. The front represents the relationship between the three objective functions: voltage RMSE, cost function, and battery throughput while tuning the predictive controller. There are 14 Pareto-optimal solutions in the Pareto front, where the value of the voltage RMSE is between 2.440 and 3.544 V, the cost function is between 1.110 and 6.776, and the battery throughput is between 0.366 and 42.197 kWh.

Moreover, from the Pareto shape it is evident that any decrease in voltage RMSE goes along with an increase in battery consumption, while the solutions with low battery consumption have a high value for voltage RMSE or do not yield good costs. This makes multi-objective optimization necessary, because otherwise one objective would be o

ptimized at the price of the other ones. So, the controller parameters are chosen from the Pareto front based on the knee-point criterion as an optimal compromise between voltage regulation, normalized cost, and battery consumption. The cost axis is a normalized optimization objective and cannot be confused with the final cost value given in Table 3 and Table 4.

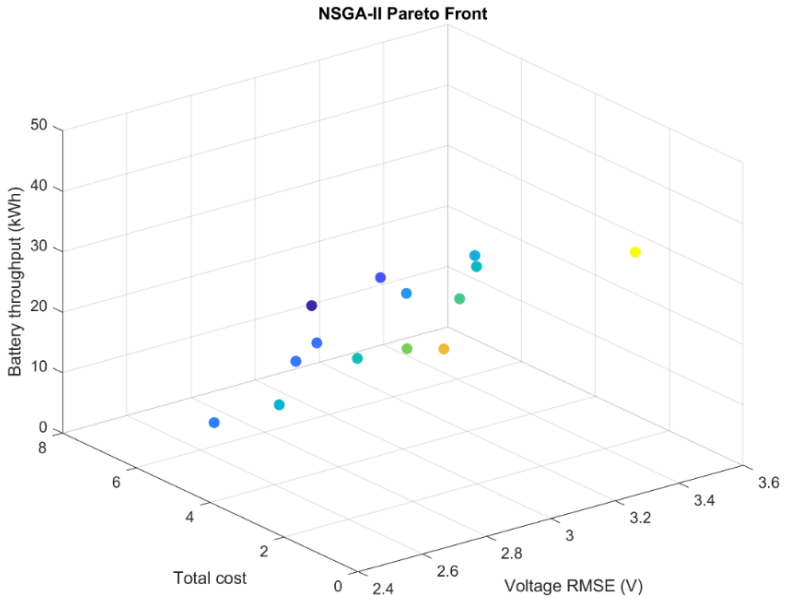


Figure 7. NSGA-II Pareto-optimal trade-offs among voltage RMSE, normalized cost, and battery throughput

4.7. Ablation Analysis

Th efollowing Figure 8 to Figure 12 and Table 6 present a sensitivity-oriented assessment of the influence of reliability-weighted fusion, learned forecasting, and continuous digital-twin support under mixed cyber-physical anomalies. As shown in Figure 8, the variant without reliability-weighted fusion produced a voltage

RMSE of 5.047 V, compared with 2.324 V for the full framework, corresponding to an observed difference of approximately 117.2%. The no-forecast and binary-replacement variants produced RMSE values of 3.205 V and 4.647 V, respectively. These results indicate that voltage-regulation performance is sensitive to the removal or replacement of the investigated components. However, because the ablation cases were generated under different random realizations, the observed differences should be interpreted as indicative performance trends rather than strict causal effects. Figure 9 further shows that the full framework did not achieve the minimum operating cost. The no-forecast variant achieved the lowest cost of 22.989, although this reduction was accompanied by poorer voltage-regulation and battery-management performance. Accordingly, the present ablation analysis is used to examine the relative sensitivity of the framework to its principal components rather than to establish a controlled statistical comparison.

The battery-related findings further showcase the benefits of the proposed full framework. As shown in Figure 10, the full proposed framework obtained the lowest battery throughput at 74.66 kWh, in comparison to 91.38 kWh without reliability fusion, 158.74 kWh without learned forecasting, and 122.97 kWh with binary replacement. Likewise, as seen in Figure 11, the proposed full framework kept the SOC violation rate at a minimal 0.83%, in contrast to the higher rates of 14.17%, 40.00%, and 38.06% of the three ablated setups, respectively. Finally, as highlighted in Figure 12, the full framework obtained the highest F1 score at 0.687 for anomaly detection, compared to 0.674 without reliability fusion, 0.624 without learned forecasting, and 0.669 with binary replacement.

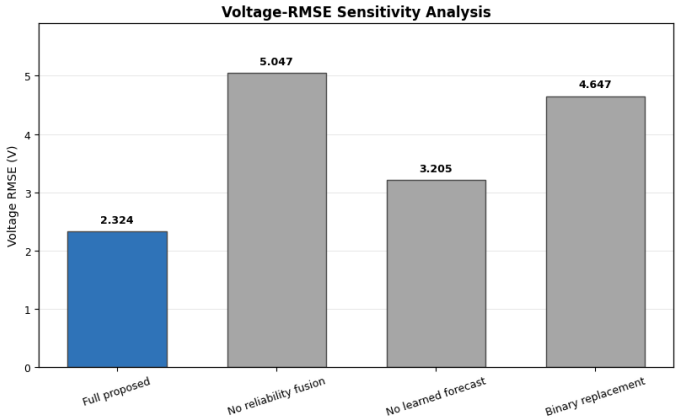


Figure 8. Sensitivity-oriented comparison of voltage RMSE among framework variants under mixed cyber-physical anomalies

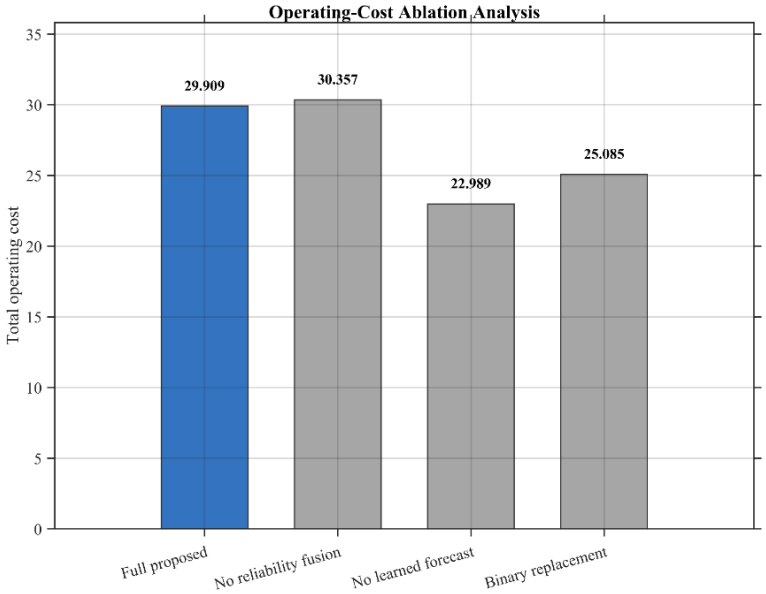


Figure 9. Operating-cost ablation analysis under the mixed cyber-physical anomaly scenario

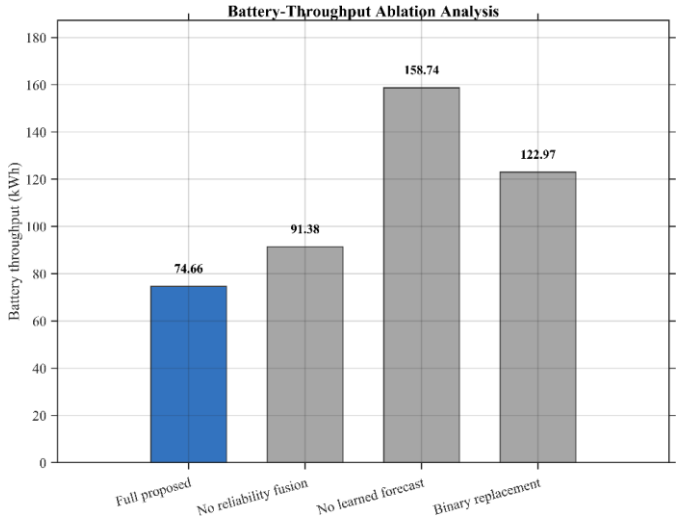


Figure 10. Battery-throughput ablation analysis under the mixed cyber-physical anomaly scenario

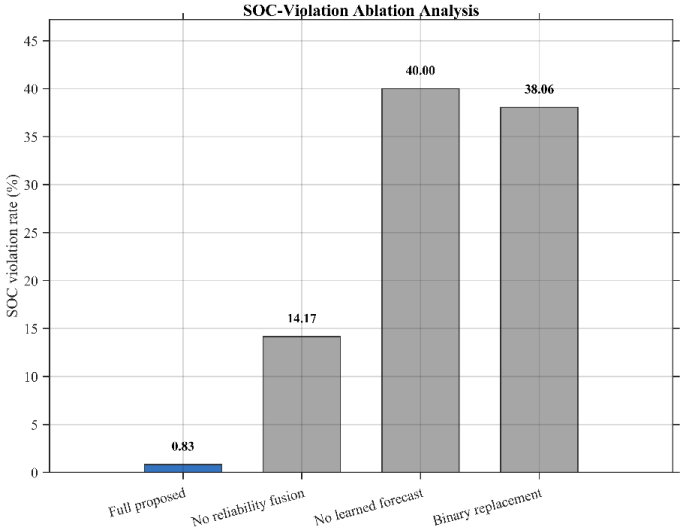


Figure 11. SOC-violation-rate ablation analysis under the mixed cyber-physical anomaly scenario

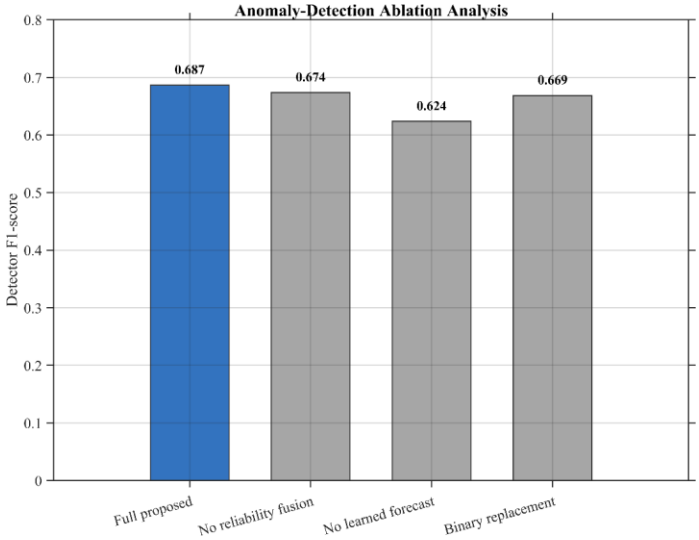


Figure 12. Anomaly-detection F1-score ablation analysis under the mixed cyber-physical anomaly scenario

These results indicate that it is not possible to attribute the performance enhancement solely to the digital twin model. It rather arises due to the synergistic interaction between forecasting, reliability estimation of the channels, and virtual state support. Specifically, the lower performance observed for the binary replacement indicates that handing over all control responsibility to the digital twin can lead to the deterioration of the system performance in the case of errors in modelling/parameter estimation in the virtual model.

The ablation results in Table 6 are treated as a sensitivity-based evaluation of the main framework components rather than as a strict statistical comparison. Since the individual cases were obtained from different random realizations, the reported values are used to show the general performance trends that occur when a specific component is removed or replaced, rather than to claim a definitive causal effect. Even with this limitation, Table 6 still provides useful information about the relative influence of reliability-weighted fusion, learned forecasting, and binary measurement replacement on voltage regulation, operating cost, battery utilization, SOC violations, and anomaly-detection performance.

Table 6. Ablation results under mixed anomalies

Variant	Voltage RMSE (V)	Total cost	Battery throughput (kWh)	SOC violation (%)	Detector F1
Full proposed framework	2.324	29.909	74.658	0.833	0.687
No reliability fusion	5.047	30.357	91.379	14.167	0.674
No learned forecast	3.205	22.989	158.743	40.000	0.624
Binary replacement	4.647	25.085	122.974	38.056	0.669

4.8. Comparative Performance Analysis

A comprehensive comparison was conducted among the rule-based controller, conventional MPC, Forecast-MPC, DT-MPC with binary measurement replacement, and the proposed reliability-weighted digital-twin MPC. The comparison considered voltage regulation, operating cost, battery utilization, anomaly-detection performance, renewable-energy utilization, and computational latency. Figure 13 to Figure 18 provide the corresponding editable graphical comparisons.

As shown in Figure 13, the proposed method achieved the lowest aggregate voltage RMSE of 1.561 V. This result represents reductions of 22.57%, 27.69%, 33.01%, and 51.28% compared with the rule-based, MPC, Forecast-MPC, and DT-MPC approaches, respectively. The proposed controller also produced the highest mean anomaly-detection F1-score of 0.312, while maintaining a 95th-percentile computational latency of 2.422 ms. These results demonstrate that the additional digital-twin estimation and reliability-fusion operations did not impose excessive computational requirements.

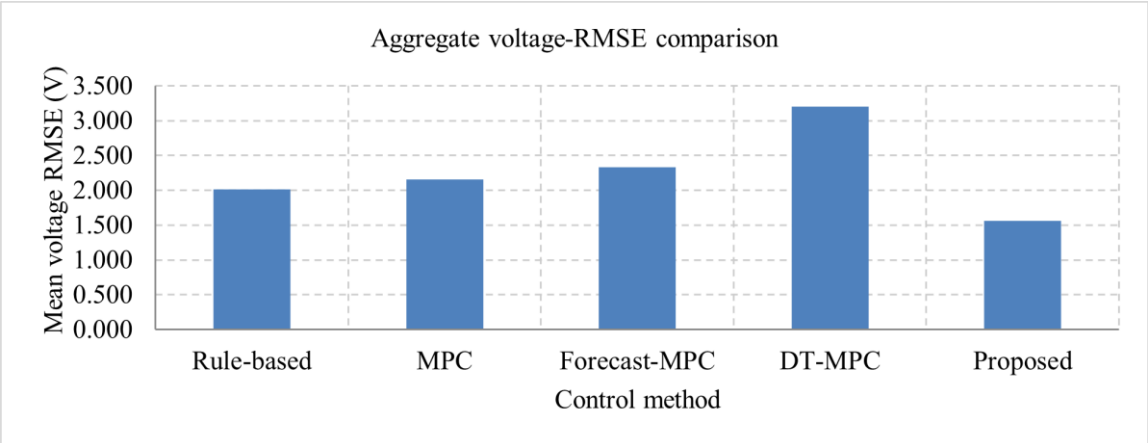


Figure 13. Aggregate voltage-regulation performance

The operating-cost comparison in the following Figure 14 demonstrates that the Forecast-MPC is able to achieved the lowest average cost of 23.801, whereas the proposed method obtained 28.814. Although the proposed controller was approximately 21.06% more expensive than Forecast-MPC, its cost remained 8.82% lower than that of the rule-based method. Moreover, the proposed battery throughput was 88.458 kWh, which was approximately 33.97% lower than the 133.976 kWh recorded by Forecast-MPC. Therefore, the resilience improvement of the proposed method was not achieved through excessive battery cycling alone.

Figure 15 shows the comparison of the results scenario-wise where the standard MPC system outperformed in terms of nominal and cloud-load cases, providing RMSE of voltage equal to 0.296 V and

0.287 V, respectively. However, for the same cases, the proposed MPC system provided results of 0.391 V and 2.338 V. The lower performance in the latter case is attributed to the rapid changes in physics being equivalent to abnormal measurements and affecting the reliability of the measurement.

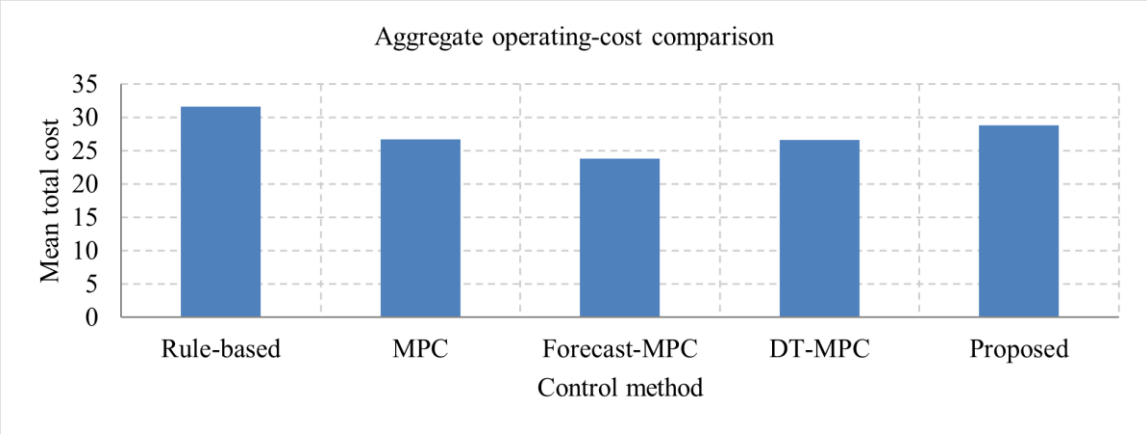


Figure 14. Comparative operating-cost performance

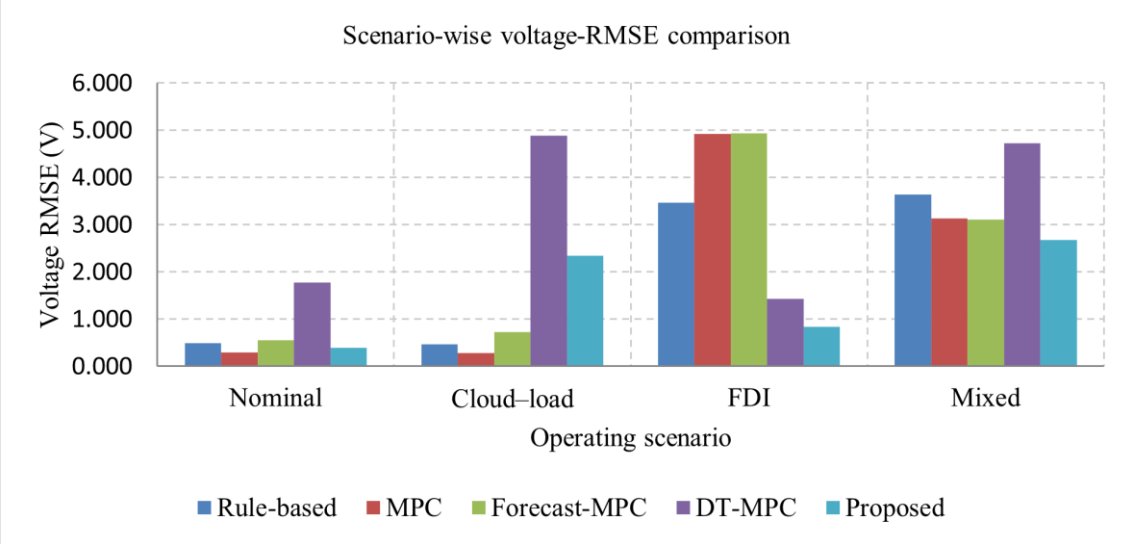


Figure 15. Scenario-wise voltage RMSE

Under the FDI scenario, the proposed framework achieved its strongest comparative improvement. Its voltage RMSE decreased to 0.843 V, compared with 4.926 V for MPC, 4.934 V for Forecast-MPC, and 1.435 V for DT-MPC. These results correspond to reductions of 82.89%, 82.92%, and 41.28%, respectively. The proposed method also achieved the highest FDI F1-score of 0.564, with a recall of 0.959, demonstrating that continuous reliability weighting effectively limited the influence of corrupted sensor measurements.

Similarly, under mixed cyber-physical anomalies, the proposed controller showed the lowest voltage RMSE value of 2.674V, which implies 26.64% improvement over rule-based control, 14.56% improvement over MPC, 13.96% improvement over Forecast-MPC, and 43.39% improvement over DT-MPC. It also had the highest F1-score of 0.684, with a recall of 0.909. As shown in Figure 16, the proposed approach not only provided better detection performance but also offered the best voltage regulation performance under the mixed anomaly. Nevertheless, it is a notable drawback that the relatively high false-alarm rate under both FDI and mixed anomalies, i.e., 0.363 and 0.434, respectively.

The normalized radar chart comparison of this study is provided in the next Figure 17 with a multi-criteria evaluation of the compared controllers. All criteria have been scaled to the range from 0 to 100 with larger values being better. The proposed control technique attained the highest normalized values for voltage regulation and anomaly detection, whereas Forecast-MPC had the highest score for cost efficiency. Rule-based control had the best relative values for battery saving and renewable energy utilization. As a result, the radar

chart proves that there is no single technique dominating all performance criteria. Still, the proposed control technique has the most balanced set of values considering anomaly-resilient voltage regulation as the main criterion.

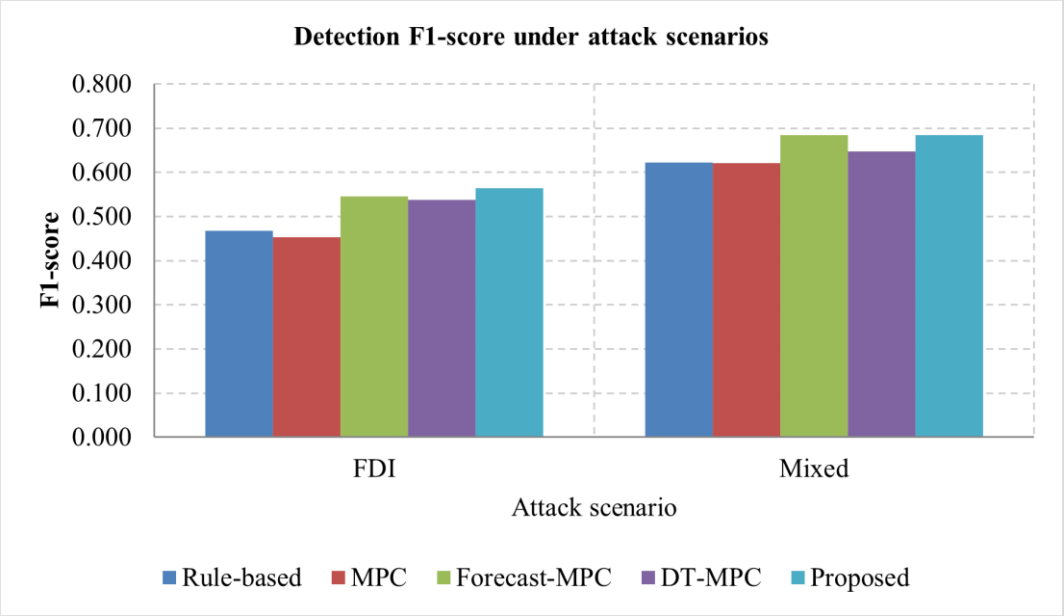


Figure 16. Attack-Detection F1 Performance

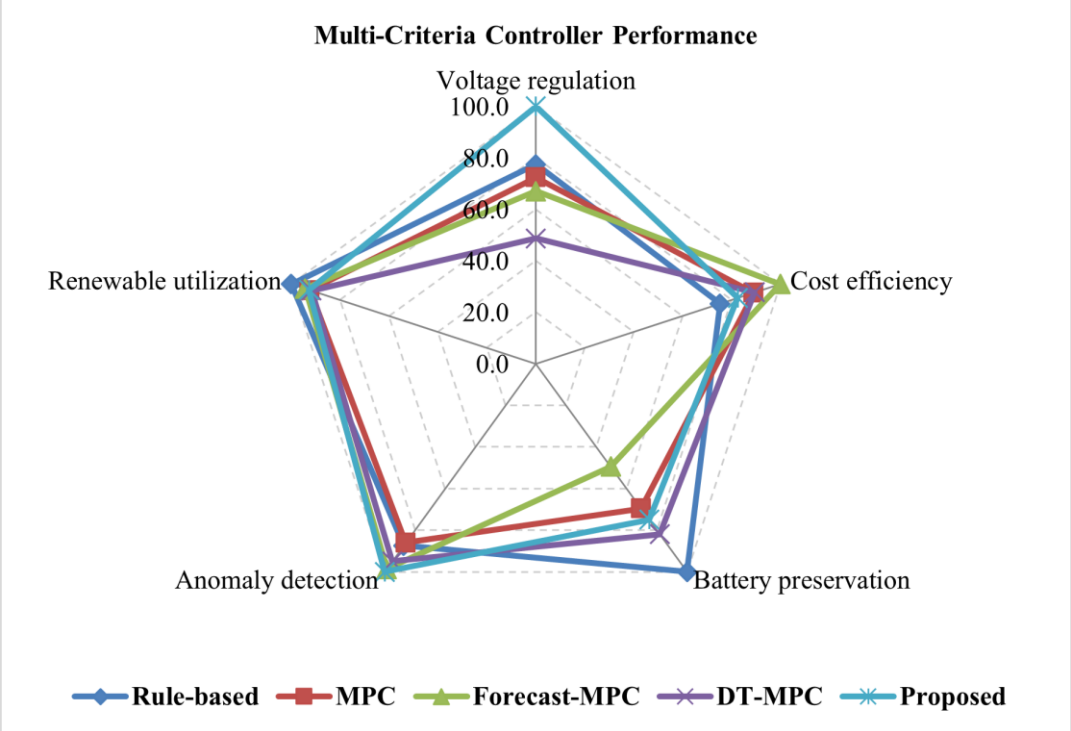


Figure 17. Multi-criteria controller performance

Moreover, the ablation study illustrated in Figure 18 also supports the impact of the components discussed above. In the ablation test conducted under the condition of mixed anomalies, the entire architecture had a voltage RMSE of 2.324 V. The removal of reliability-weighted fusion led to a rise in the RMSE to 5.047 V, whereas the removal of forecasting learning led to an increase in the RMSE to 3.205 V. Similarly, binary

measurement substitution led to an increase in the RMSE to 4.647 V. Besides, the entire framework generated the lowest SOC violation rate of 0.833% and the lowest battery throughput of 74.658 kWh.

Completely, the comparison demonstrates that the proposed framework is not universally superior under all operating conditions. Conventional MPC remains more effective during nominal and rapid cloud–load variations, while Forecast-MPC provides the lowest operating cost. However, the proposed method clearly provides the strongest performance when measurements are corrupted by FDI or mixed cyber-physical anomalies. Its principal benefit is therefore improved anomaly-resilient voltage regulation with practical real-time computational performance, rather than unconditional superiority across every economic and operational criterion.

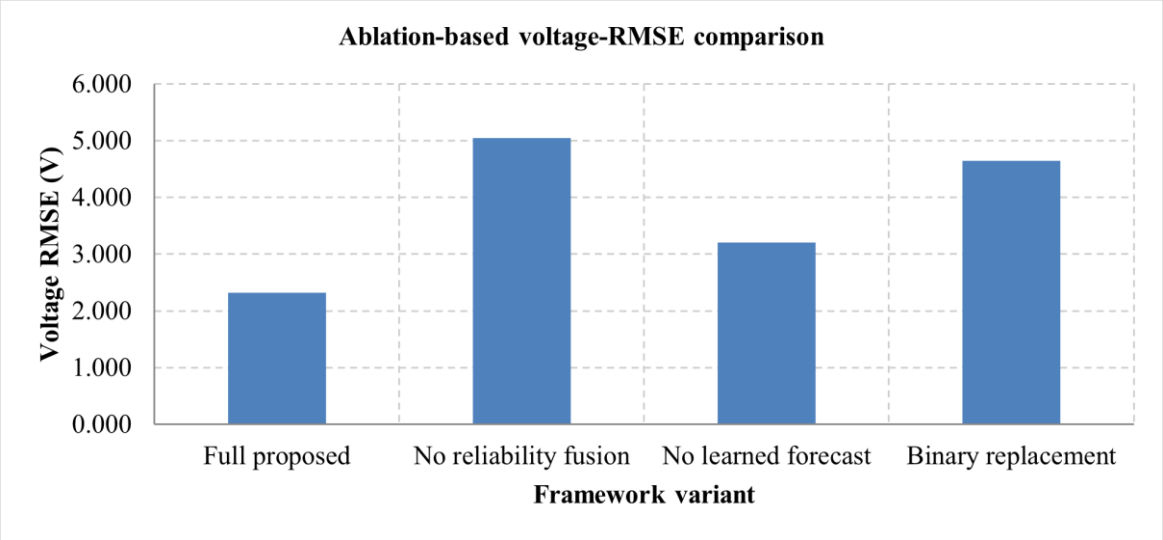


Figure 18. Ablation-Based Performance Evaluation

4.9. Network and Edge-Computing Performance

To evaluate the computational suitability of the proposed framework for deployment within an IoT-enabled edge–cloud architecture, the local runtime performance of the predictive controllers was assessed using the 95th-percentile (P95) edge-processing latency and the predictive-optimization success rate. As shown in the following Table 7 and Figure 19, the proposed controller achieved a P95 local edge-processing latency of 2.422 ms, compared with 2.673 ms for conventional MPC and 2.517 ms for DT-MPC. Forecast-MPC achieved the lowest latency at 2.369 ms, while the proposed framework introduced only a 0.053 ms increase, corresponding to approximately 2.24%. Based on the measured local processing latency, the proposed method provides a theoretical sequential computational capacity of approximately 413 control updates per second. This value represents the maximum local algorithmic processing rate and excludes communication-related delays associated with propagation, transmission, queuing, synchronization, packet retransmission, and actuator response.

The MPC solver retained an approximate success rate of 99.86%, implying steady execution in real time despite the extra computation for anomaly scores, channel-wise reliability analysis, and digital twin integration. As can be seen from Figure 20, the proposed approach has been able to obtain the minimum aggregate voltage RMSE of 1.561 V among all the other predictive control methods. Even though the Forecast-MPC has lower latency in the P95 percentile of 2.369 ms, it has obtained a greater aggregate voltage RMSE of 2.331 V. Thus, the overall performance demonstrated in Figure 19 and Figure 20 is a strong trade-off between voltage regulation and computational speed.

It is necessary to declare that P95 latency represents local algorithmic processing time at the edge and does not include communication propagation, transmission, queuing, retransmission, synchronization, or actuator-response delays.

However, this latency is an indicator of local processing latency of the algorithm rather than total network latency. Future hardware-in-the-loop and communication network co-simulations need to study packet losses, propagation and queuing delays, communication jitters, bandwidth limitations, overhead associated with retransmission of packets, synchronization issues, and age-of-information.

Table 7. Edge-processing performance of the predictive control methods

Performance indicator	MPC	Forecast-MPC	DT-MPC	Proposed
P95 edge-processing latency (ms)	2.673	2.369	2.517	2.422
Theoretical sequential processing capacity (updates/s)	374.1	422.1	397.3	412.9
Predictive-optimization success rate (%)	-	-	-	≈99.86

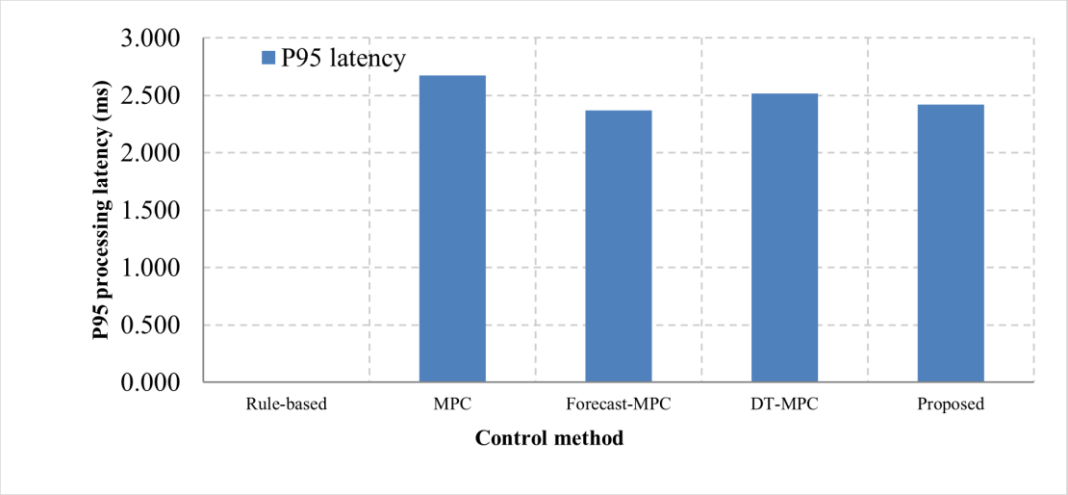


Figure 19. Comparison of the 95th-percentile processing latency among the predictive control methods

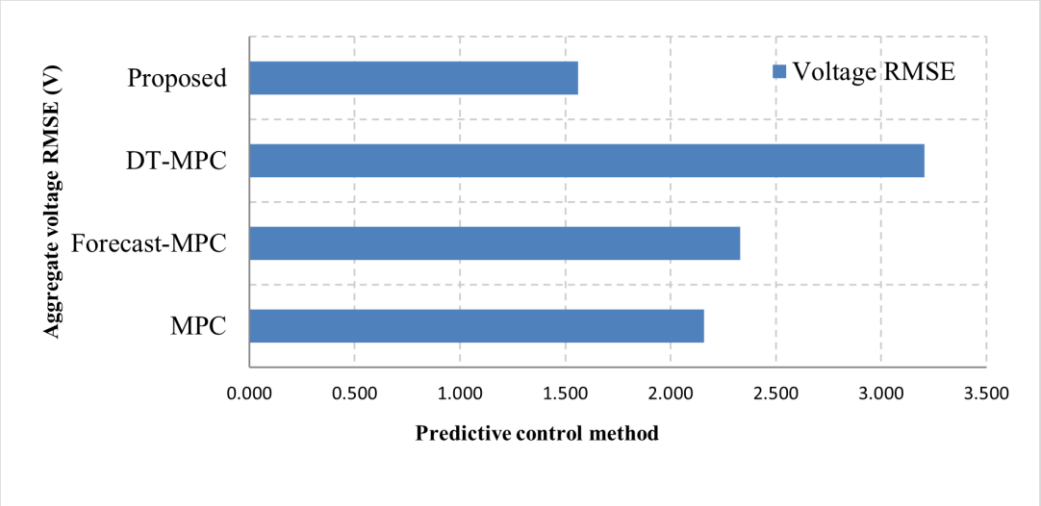


Figure 20. Aggregate voltage-RMSE comparison among the predictive control methods

4.10. IoT, Network, and Edge-Computing Performance

From an IoT deployment perspective, the obtained processing results demonstrate that the proposed framework can be executed at an edge gateway connected to distributed smart meters, environmental sensors, battery-management units, converter-monitoring devices, and communication-status nodes. The proposed controller achieved a 95th-percentile edge-processing latency of 2.422 ms, corresponding to a theoretical sequential processing capacity of approximately 413 control updates per second. This capacity represents the maximum algorithmic processing rate and excludes communication propagation, queuing, synchronization, packet retransmission, and actuator-response delays. The proposed method was approximately 9.39% faster than conventional MPC and 3.77% faster than DT-MPC, while its latency was only 0.053 ms, or approximately 2.24%, higher than that of Forecast-MPC. Therefore, the additional anomaly scoring, channel-wise reliability evaluation, and digital-twin fusion operations introduced only a marginal computational overhead. Together with an MPC solver success rate of approximately 99.86%, these findings support the feasibility of deploying the online control functions at an edge-computing gateway rather than relying exclusively on remote cloud execution.

The results also demonstrate the role of the proposed framework in protecting IoT-delivered measurement streams. Under false-data injection, the proposed method reduced the voltage RMSE to 0.843 V and achieved an anomaly-detection recall of 0.959. Under mixed cyber-physical anomalies, it maintained the lowest voltage RMSE of 2.674 V and an F1-score of 0.684. These results indicate that reliability-weighted fusion can reduce the influence of corrupted measurements received through the microgrid communication infrastructure before they are used by the predictive controller. The resilience demonstrated in this study is therefore related to measurement integrity and trusted-state construction within a networked microgrid environment, rather than to end-to-end communication-network resilience or the performance of a specific wired or wireless communication protocol.

The task allocation for the edge-cloud architecture further helps in implementing the proposed system in a scalable manner. The time-critical tasks such as filtering, synchronization, residual generation, anomaly detection, reliability assessment, state fusion, and MPC control calculation are allocated to the edge gateway. The computationally demanding tasks like storage of big data, training of machine learning models, Bayesian optimization, tuning of PSO-based detector, optimization of the controller via NSGA-II, and the digital twin updating are allocated to the cloud tier. Updated models and optimal parameter sets are sent to the edge controller from the cloud, and trusted states, alarms, and performance data can be sent to the cloud from the edge as mentioned in Table 8.

The latency cited pertains solely to the latency incurred in the execution of the algorithm locally and is not the total end-to-end network latency. In this case study, parameters relating to the performance of the algorithm on the network level like the packet delivery ratio, bandwidth utilization, communication jitter, propagation and queuing latency, retransmission latency, energy utilization by the wireless node, and protocol behavior have not been tested empirically. Such research needs to be done in future studies.

Table 8. IoT and edge-computing interpretation of the existing results

Indicator	Proposed value	IoT/network interpretation
P95 edge-processing latency	2.422 ms	Low-latency edge execution
Theoretical sequential capacity	≈413 updates/s	Maximum local algorithmic processing rate
MPC solver success rate	≈99.86%	Stable online optimization
Latency reduction relative to MPC	9.39%	Lower edge-computing burden
Latency reduction relative to DT-MPC	3.77%	Efficient digital-twin integration
Latency overhead relative to Forecast-MPC	2.24%	Small cost for anomaly resilience
FDI detection recall	0.959	High sensitivity to corrupted IoT measurements
Mixed-anomaly F1-score	0.684	Balanced detection under combined disturbances

5. COMPARATIVE ANALYSIS AND FUTURE INSIGHTS

Recent studies have addressed different aspects of intelligent and cyber-resilient microgrids, including renewable and load forecasting, digital-twin modelling, false-data-injection detection, resilient predictive control, IoT communication, and distributed network operation. Nonetheless, most of the considered papers address only a few of these aspects without including the issues of measurement reliability, digital twin state estimation, predictive control, communication awareness, and edge-cloud computation into a single approach. In order to differentiate between the approaches, Table 9 presents the most important features and numerical values obtained for each paper as well as for the current work. It should be emphasized that the discussed research works utilize various microgrids' setups, datasets, cyberattacks, assumptions regarding the communication environment, control goals, and evaluation criteria; thus, the values provided in Table 9 cannot be considered as a ranking list of performance. On the contrary, Table 9 should be seen as a quantitative comparison that illustrates the strengths and weaknesses of existing approaches and indicates the key areas of future research.

The forecasting process remains an important research direction. As proved by the research done in [44], various learning algorithms might have very similar, yet slightly different forecasting ability, with XGBoost having the best RMSE compared to other algorithms tested. However, in this case, the forecasting algorithm acts merely as a support for the prediction horizon of MPC and is not responsible for robustness against anomaly detection. Future research in this direction should be related to the investigation of ensembles of forecasts, probabilistic prediction, online model selection, and uncertainty-based MPC especially during fast irradiance changes.

The performance of communication networks is another critical direction for study. The route analysis presented in [45] showed that different routes can exhibit differences in terms of computation, throughput, and delay, while the analysis of CoAP and MQTT-SN protocols in [46] proved that protocol choice for IoT can have an impact on communication and energy needs of the nodes as well. This information is especially useful

in regard to the suggested edge-cloud micro-grid topology. Although the current model produced 2.422 ms of P95 latency for local edge processing, it only takes into account local algorithmic processing and does not account for the transmission, route, queue, retransmission, synchronization, and wireless medium latencies.

Table 9. Quantitative comparison of recent related studies and the proposed framework.

Study	Main focus	Key result	Relevance to present work
[44]	Load forecasting	XGBoost RMSE = 0.2127	Supports improvement of the forecasting layer
[45]	MANET routing	Compared routing efficiency, throughput, and delay	Relevant to communication-network design
[46]	CoAP vs MQTT-SN	Protocol-dependent differences in node power use	Highlights IoT protocol impact
[47]	Cyber-resilient DC microgrid	<1% voltage error; 1.5 ms execution time	Useful hardware-level resilience benchmark
[48]	MPC-based FDI resilience	FDI detection and recovery using MPC/Kalman estimation	Closely related resilient-MPC approach
[49]	FDIA detection	99.96% accuracy; 99.4% with sensor noise	Indicates potential for improved attack discrimination
[50]	BESS digital twin	MAPE <0.50%	Supports higher-fidelity digital-twin validation
[51]	DT-SDN cybersecurity	DT integrated with SDN and intrusion detection	Relevant to network-aware DT integration
[52]	Microgrid energy management	~60% cost reduction; ~90% loss-of-load reduction	Highlights the importance of economic performance
[53]	FDIA mitigation	Maintained operation under severe attacks	Supports improved anomaly mitigation
Present work	Reliability-weighted DT-MPC	RMSE = 1.561 V; FDI RMSE = 0.843 V; recall = 0.959; F1 = 0.684; latency = 2.422 ms	Integrates forecasting, DT, anomaly detection, MPC, and edge–cloud processing

The embedded implementation reported in [47] provides an additional reference point for real-time cyber-resilient control, where an execution time of 1.5 ms was demonstrated on an ARM Cortex-M3 platform. This result highlights the importance of validating the proposed framework on an actual edge-processing platform rather than relying only on software-level execution measurements. Closely related resilient-MPC research in [48] further demonstrates the importance of combining attack detection and control recovery within the same closed-loop framework. In comparison, the present approach introduces continuous reliability-weighted fusion between physical measurements and digital-twin estimates rather than relying only on detection and subsequent recovery.

Anomaly detection is another critical aspect where further advancements can be made. In the decentralized FDIA work presented in [49], extremely high accuracy was observed in detection during experiments, conducted under ideal as well as non-ideal measurement scenarios. Even though the experimental scenarios and types of attacks considered in the current research are different from the above, it still points towards the possibilities of achieving improvements by enhancing feature construction, adaptive thresholding, and consistency between multiple channels. This is especially true since the current system demonstrated recall scores of 0.959 and 0.909 under FDI and mixed anomaly scenarios, respectively, but resulted in false alarm ratios of 0.363 and 0.434.

A third research direction is digital-twin accuracy. According to the digital-twin paper of BESS in [50], the MAPE for digital-twin simulations was less than 0.50% through simulations on PV, microgrid, and aged batteries, thus stressing the importance of validation of virtual systems under realistic operating conditions and degradation. Moreover, the use of digital-twin techniques along with software-defined networking and cyber-security approaches in [51] shows the advantages that can be gained by merging a virtual representation of a system with network management and cyber-security capabilities. Future expansions of the current model should then include aged batteries, temperature dependent parameters, converter degradation, real-time uncertainties, and enhanced digital-twin-network integration.

Economics is another aspect that requires increased attention. The microgrid energy management framework in [52], which did not rely on forecasting for decision-making purposes, exhibited remarkable gains in operating cost and reliability. This means that the economic aspect greatly impacts the selection of the appropriate control scheme. In this research, although the framework under consideration resulted in the smallest total RMSE of voltages, the average operating cost (28.814) was approximately 21.06% higher than the value of 23.801 reported in the case of Forecast-MPC. It clearly indicates that the ability to maintain resilient to anomalies and manage the voltage level comes at the cost of economic losses.

Finally, the approach of attack detection and mitigation in [53] further highlights the possibility of using statistical and data-driven techniques to maintain microgrid stability during serious cyber-attacks. These kinds

of techniques can be used to supplement the reliability-based fusion technique proposed in this work by distinguishing actual transients from malicious attacks on system measurements. In summary, the discussion shows that the development of the framework should focus on the integration of all factors, including forecasting, communication network, digital twin technology, detection, predictive control, and economics.

6. CONCLUSION

The proposed AI-driven big-data digital-twin framework with network-aware MPC provides an integrated solution for improving the resilience of PV–battery microgrids operating within IoT-enabled edge–cloud environments. The framework combines electrical, environmental, battery, and communication-status information with edge-based preprocessing, anomaly detection, reliability assessment, trusted-state construction, and predictive control. Cloud resources are used for historical data storage, forecasting-model training, digital-twin refinement, and optimization. The main contribution of the framework is the continuous reliability-weighted fusion of physical measurements and digital-twin estimates, which limits the effect of corrupted IoT measurements without relying on abrupt binary replacement. The proposed method achieved the lowest aggregate voltage RMSE of 1.561 V and showed its clearest advantages when measurement integrity was degraded. Under false-data injection, the voltage RMSE was reduced to 0.843 V with a detection recall of 0.959, while under mixed cyber-physical anomalies the framework achieved an RMSE of 2.674 V and an F1-score of 0.684. These findings show that the main resilience improvement is associated with reliability-aware trusted-state construction and digital-twin support rather than with the forecasting layer alone. This distinction is important because the PV forecasting model showed limited accuracy during rapid irradiance changes, and conventional MPC remained more effective under some nominal and cloud–load conditions. In addition, Forecast-MPC achieved a lower average operating cost, indicating that the improvements in resilience and voltage regulation involve an economic trade-off. The relatively high false-alarm rates also remain a limitation that should be addressed through further detector refinement. From an IoT and communication perspective, the proposed controller achieved a 95th-percentile edge-processing latency of 2.422 ms, a theoretical local processing capacity of approximately 413 updates/s, and a solver success rate of about 99.86%. These results indicate that the online control functions can be executed with low computational delay at the edge. However, this latency represents local algorithmic processing time rather than complete end-to-end network performance. Packet-delivery ratio, communication jitter, bandwidth consumption, retransmission overhead, queuing delay, synchronization errors, and protocol-specific behavior were not experimentally evaluated. Future work should therefore focus on improving PV forecasting accuracy, reducing false alarms, strengthening online digital-twin adaptation, and validating the proposed framework through hardware-in-the-loop experiments and communication-network co-simulation under realistic IoT protocols, packet-loss conditions, wireless constraints, and end-to-end network delays.

Author Contribution

All authors contributed equally to the main contributor to this paper. All authors read and approved the final paper.

Conflicts of Interest

The authors declare no conflict of interest.

REFERENCES

[1] M. Uddin, H. Mo, D. Dong, S. Elsawah, J. Zhu, and J. M. Guerrero, "Microgrids: A review, outstanding issues and future trends," *Energy Strategy Rev.*, vol. 49, p. 101127, 2023, https://doi.org/10.1016/j.esr.2023.101127.

[2] M. S. Alam, M. A. Hossain, M. Shafiullah, A. Islam, M. S. H. Choudhury, M. O. Faruque, and M. A. Abido, "Renewable energy integration with DC microgrids: Challenges and opportunities," *Electr. Power Syst. Res.*, vol. 234, p. 110548, 2024, https://doi.org/10.1016/j.epsr.2024.110548.

[3] X. Zhang, Z. Zhang, R. Zhang, W. Liu, H. Li, and J. Peng, "Event-triggered resilient recovery learning control protocol for interconnected DC microgrids with distributed attack detection," *Sustain. Energy Grids Netw.*, vol. 38, p. 101364, 2024, https://doi.org/10.1016/j.segan.2024.101364.

[4] S. M. Miraftabzadeh and M. Longo, "High-resolution PV power prediction model based on the deep learning and attention mechanism," *Sustain. Energy Grids Netw.*, vol. 34, p. 101025, 2023, https://doi.org/10.1016/j.segan.2023.101025.

[5] R. Fallahifar and M. Kalantar, "Optimal planning of lithium ion battery energy storage for microgrid applications: Considering capacity degradation," *J. Energy Storage*, vol. 57, p. 106103, 2023, https://doi.org/10.1016/j.est.2022.106103.

[6] C. Zhong, H. Zhao, Y. Liu, and C. Liu, "Learning-based model predictive secondary frequency control of PV-ESS-EV microgrid," *Int. J. Electr. Power Energy Syst.*, vol. 159, p. 110020, 2024, https://doi.org/10.1016/j.ijepes.2024.110020.
[7] I. Natgunanathan, V. Mak, S. Rajasegarar, and A. Anwar, "Deakin microgrid digital twin and analysis of AI models for power generation prediction," *Energy Convers. Manage.: X*, vol. 18, p. 100370, 2023, https://doi.org/10.1016/j.ecmx.2023.100370.
[8] H. M. Marhoon *et al.*, "Microcontroller-based internet of things control system for autonomous hidden camera detection using adaptive decision-making and hybrid MCDM techniques," *Discov. Comput.*, vol. 29, p. 584, 2026, https://doi.org/10.1007/s10791-026-10480-8.
[9] H. Li, Y. Yang, Y. Liu, and W. Pei, "Federated dueling DQN based microgrid energy management strategy in edge-cloud computing environment," *Sustain. Energy Grids Netw.*, vol. 38, p. 101329, 2024, https://doi.org/10.1016/j.segan.2024.101329.
[10] Q. Xia, Y. Wang, Y. Zou, Z. Yan, N. Zhou, Y. Chi, and Q. Wang, "Regional-privacy-preserving operation of networked microgrids: Edge-cloud cooperative learning with differentiated policies," *Appl. Energy*, vol. 370, p. 123611, 2024, https://doi.org/10.1016/j.apenergy.2024.123611.
[11] K. Kumar, P. Kumar, S. Kar, and A. K. Bohre, "Anomaly detection technique for securing microgrid against false data attacks," *ISA Trans.*, vol. 153, pp. 13–27, 2024, https://doi.org/10.1016/j.isatra.2024.07.037.
[12] M. Pan, Q. Xing, Z. Chai, H. Zhao, Q. Sun, and D. Duan, "Real-time digital twin machine learning-based cost minimization model for renewable-based microgrids considering uncertainty," *Sol. Energy*, vol. 250, pp. 355–367, 2023, https://doi.org/10.1016/j.solener.2023.01.006.
[13] K. Bitirgen and Ü. B. Filik, "A hybrid deep learning model for discrimination of physical disturbance and cyber-attack detection in smart grid," *Int. J. Crit. Infrastruct. Prot.*, vol. 40, p. 100582, 2023, https://doi.org/10.1016/j.ijcip.2022.100582.
[14] Z. Lu, Y. Gao, C. Xu, and Y. Li, "Configuration optimization of an off-grid multi-energy microgrid based on modified NSGA-II and order relation-TODIM considering uncertainties of renewable energy and load," *J. Clean. Prod.*, vol. 383, p. 135312, 2023, https://doi.org/10.1016/j.jclepro.2022.135312.
[15] E. O'Dwyer, I. Pan, R. Charlesworth, S. Butler, and N. Shah, "Integration of an energy management tool and digital twin for coordination and control of multi-vector smart energy systems," *Sustain. Cities Soc.*, vol. 62, p. 102412, 2020, https://doi.org/10.1016/j.scs.2020.102412.
[16] R. K. Gupta, F. Sossan, and M. Paolone, "Grid-aware distributed model predictive control of heterogeneous resources in a distribution network: Theory and experimental validation," *IEEE Trans. Energy Convers.*, vol. 36, no. 2, pp. 1392–1402, 2021, https://doi.org/10.1109/TEC.2020.3015271.
[17] C. Semeraro, M. Lezoche, H. Panetto, and M. Dassisti, "Digital twin paradigm: A systematic literature review," *Comput. Ind.*, vol. 130, p. 103469, 2021, https://doi.org/10.1016/j.compind.2021.103469.
[18] Y. Li, X. Wei, Y. Li, Z. Dong, and M. Shahidehpour, "Detection of false data injection attacks in smart grid: A secure federated deep learning approach," *IEEE Trans. Smart Grid*, vol. 13, no. 6, pp. 4862–4872, 2022, https://doi.org/10.1109/TSG.2022.3204796.
[19] A. Othman, G. Kaddoum, J. V. C. Evangelista, M. Au, and B. L. Agba, "Digital twinning in smart grid networks: Interplay, resource allocation and use cases," *IEEE Commun. Mag.*, vol. 61, no. 11, pp. 120–126, 2023, https://doi.org/10.1109/MCOM.001.2200823.
[20] N. Qi, K. Huang, Z. Fan, and B. Xu, "Long-term energy management for microgrid with hybrid hydrogen-battery energy storage: A prediction-free coordinated optimization framework," *Appl. Energy*, vol. 377, p. 124485, 2025, https://doi.org/10.1016/j.apenergy.2024.124485.
[21] K. Huang, L. Cheng, N. Qi, D. W. Gao, A. Mujeeb, and Q. Guo, "Grid-aware real-time dispatch of microgrid with generalized energy storage: A prediction-free online optimization approach," *IEEE Trans. Smart Grid*, vol. 17, no. 2, pp. 892–909, 2026, https://doi.org/10.1109/TSG.2025.3627407.
[22] N. Doumèche, Y. Allioux, Y. Goude, and S. Rubrichi, "Human spatial dynamics for electricity demand forecasting: The case of France during the 2022 energy crisis," *IEEE Trans. Power Syst.*, vol. 41, no. 3, pp. 1882–1891, 2026, https://doi.org/10.1109/TPWRS.2025.3648653.
[23] E. D. Ayele, J. F. Gonzalez, and W. B. Teeuw, "Enhancing cybersecurity in distributed microgrids: A review of communication protocols and standards," *Sensors*, vol. 24, no. 3, p. 854, 2024, https://doi.org/10.3390/s24030854.
[24] G. P. Reddy, Y. V. P. Kumar, and M. K. Chakravarthi, "Communication technologies for interoperable smart microgrids in urban energy community: A broad review of the state of the art, challenges, and research perspectives," *Sensors*, vol. 22, no. 15, p. 5881, 2022, https://doi.org/10.3390/s22155881.
[25] Y.-S. Lee and C. Wang, "A cyber-physical testbed for IoT microgrid design and validation," *Electronics*, vol. 13, no. 7, p. 1181, 2024, https://doi.org/10.3390/electronics13071181.
[26] O. Ali, T.-L. Nguyen, and O. A. Mohammed, "Assessment of cyber-physical inverter-based microgrid control performance under communication delay and cyber-attacks," *Appl. Sci.*, vol. 14, no. 3, p. 997, 2024, https://doi.org/10.3390/app14030997.
[27] I. Kharchouf and O. A. Mohammed, "Controller hardware-in-the-loop testbed of a distributed consensus multi-agent system control under deception and disruption cyber-attacks," *Energies*, vol. 17, no. 7, p. 1669, 2024, https://doi.org/10.3390/en17071669.

[28] M. S. Abdelrahman, I. Kharchouf, H. M. Hussein, M. Essofally, and O. A. Mohammed, "Enhancing cyber-physical resiliency of microgrid control under denial-of-service attack with digital twins," *Energies*, vol. 17, no. 16, p. 3927, 2024, https://doi.org/10.3390/en17163927.
[29] S. Shin, M. Park, T. Kim, and H. Yang, "Architecture for enhancing communication security with RBAC IoT protocol-based microgrids," *Sensors*, vol. 24, no. 18, p. 6000, 2024, https://doi.org/10.3390/s24186000.
[30] M. A. Taher, M. Tariq, and A. I. Sarwat, "Trust-based detection and mitigation of cyber attacks in distributed cooperative control of islanded AC microgrids," *Electronics*, vol. 13, no. 18, p. 3692, 2024, https://doi.org/10.3390/electronics13183692.
[31] Y. Chen, K. Hayawi, M. Fan, S. Y. Chang, J. Tang, L. Yang, R. Zhao, Z. Mao, and H. Wen, "A bilevel optimization model based on edge computing for microgrid," *Sensors*, vol. 22, no. 20, p. 7710, 2022, https://doi.org/10.3390/s22207710.
[32] L. Zhang, C. Liu, B. Li, H. Fang, and J. Gu, "A secure storage and deletion verification scheme of microgrid data based on integrating blockchain into edge computing," *Electronics*, vol. 11, no. 23, p. 4033, 2022, https://doi.org/10.3390/electronics11234033.
[33] E. Yaghoubi, E. Yaghoubi, Z. Yusupov, and M. R. Maghami, "A real-time and online dynamic reconfiguration against cyber-attacks to enhance security and cost-efficiency in smart power microgrids using deep learning," *Technologies*, vol. 12, no. 10, p. 197, 2024, https://doi.org/10.3390/technologies12100197.
[34] N. Kumari, A. Sharma, B. Tran, N. Chilamkurti, and D. Alahakoon, "A comprehensive review of digital twin technology for grid-connected microgrid systems: State of the art, potential and challenges faced," *Energies*, vol. 16, no. 14, p. 5525, 2023, https://doi.org/10.3390/en16145525.
[35] B. Sahoo, S. Panda, P. K. Rout, M. Bajaj, and V. Blazek, "Digital twin enabled smart microgrid system for complete automation: An overview," *Results Eng.*, vol. 25, p. 104010, 2025, https://doi.org/10.1016/j.rineng.2025.104010.
[36] M. M. H. Sifat, S. M. Choudhury, S. K. Das, H. Pota, and F. Yang, "Novel abstractions and experimental validation for digital twin microgrid design: Lab scale studies and large scale proposals," *Appl. Energy*, vol. 377, p. 124621, 2025, https://doi.org/10.1016/j.apenergy.2024.124621.
[37] B. Canaan, Y. Makhlouf, and D. Ould Abdeslam, "Cyber-physical security for microgrids through digital twin technologies: A review and research outlook," *Energy Convers. Manage.: X*, vol. 28, p. 101406, 2025, https://doi.org/10.1016/j.ecmx.2025.101406.
[38] D. Salaorni, F. Bianchi, S. Colnago, A. Barisione, F. Trovò, and M. Restelli, "A novel digital twin for battery energy storage systems in micro-grids," *J. Energy Storage*, vol. 132, p. 117745, 2025, https://doi.org/10.1016/j.est.2025.117745.
[39] I. Poonahela, A. Krama, S. Bayhan, U. Fesli, M. B. Shadmand, H. Abu-Rub, and M. M. Begovic, "Hierarchical model-predictive droop control for voltage and frequency restoration in AC microgrids," *IEEE Open J. Ind. Electron. Soc.*, vol. 4, pp. 85–97, 2023, https://doi.org/10.1109/OJIES.2023.3240070.
[40] M. Jamali, M. S. Sadabadi, M. Davari, S. Sahoo, and F. Blaabjerg, "Resilient cooperative secondary control of islanded AC microgrids utilizing inverter-based resources against state-dependent false data injection attacks," *IEEE Trans. Ind. Electron.*, vol. 71, no. 5, pp. 4719–4730, 2024, https://doi.org/10.1109/TIE.2023.3281698.
[41] S. Hussain, S. M. S. Hussain, M. Hemmati, A. Iqbal, R. Alammari, S. Zanero, E. Ragaini, and G. Gruosso, "A novel hybrid cybersecurity scheme against false data injection attacks in automated power systems," *Prot. Control Mod. Power Syst.*, vol. 8, p. 37, 2023, https://doi.org/10.1186/s41601-023-00312-y.
[42] K. A. Haque, M. Massaoudi, L. Al Homoud, K. R. Davis, M. Kabalan, and H. Salamy, "Cyber-physical emulation and threat scenario simulation for enhanced microgrid resilience," *IEEE Access*, vol. 13, pp. 101455–101471, 2025, https://doi.org/10.1109/ACCESS.2025.3578421.
[43] N. E. M. Barreto and A. R. Aoki, "Cyber-physical power system digital twins—A study on the state of the art," *Energies*, vol. 18, no. 22, p. 5960, 2025, https://doi.org/10.3390/en18225960.
[44] N. Basil, N. Cherif, M. B. Alhamadani, H. Hasan, and T. F. Agajie, "Comparative analysis of LSTM, HHOSOA, COAESPSO, and XGBoost models for time series load forecasting," *Int. J. Comput. Eng. Artif. Intell. (IJCEAI)*, vol. 1, no. 1, pp. 10–22, 2026, https://ijceai.org/index.php/ijceai/article/view/13.
[45] D. B. Aeggegn and S. D. Hamdi, "Comparative performance analysis of Dijkstra, Bellman-Ford, and Floyd-Warshall routing algorithms in MANETs," *Int. J. Smart Control Electr. Eng. Syst.*, vol. 1, no. 1, pp. 22–29, 2026, https://ijscees.org/index.php/pub/article/view/10.
[46] R. A. Al-Qassab and M. I. Aal-Nouman, "Performance evaluation of CoAP and MQTT_SN protocols," in *Emerging Technology Trends in Internet of Things and Computing*, ser. Commun. Comput. Inf. Sci., vol. 1548. Cham, Switzerland: Springer, 2022, pp. 223–236, https://doi.org/10.1007/978-3-030-97255-4_17.
[47] P. M. Khan, S. Madichetty, S. S. Koduru, S. P. Machina, and S. Mishra, "Cyber-resilient DC microgrids: PINN-based control framework against false data injection attacks," *Sustain. Comput. Inform. Syst.*, vol. 51, p. 101395, 2026, https://doi.org/10.1016/j.suscom.2026.101395.
[48] R. Nandi, M. Tripathy, C. P. Gupta, and R. Singh, "MPC-based detection and resilience against bounded and unbounded FDI cyberattacks in isolated AC microgrid with battery-source DERs," *Sustain. Energy Grids Netw.*, vol. 43, p. 101719, 2025, https://doi.org/10.1016/j.segan.2025.101719.
[49] O. Danaei, S. Karimi, K. M. Almustafa, and J. Katrib, "Decentralized detection and mitigation of false data injection attacks in DC microgrids using artificial neural network," *IEEE Access*, vol. 13, pp. 136002–136015, 2025, https://doi.org/10.1109/ACCESS.2025.3594245.

[50] D. Salaorni, F. Bianchi, S. Colnago, A. Barisione, F. Trovò, and M. Restelli, "A novel digital twin for battery energy storage systems in micro-grids," *J. Energy Storage*, vol. 132, p. 117745, 2025, https://doi.org/10.1016/j.est.2025.117745.
[51] P. Kumar, R. Kumar, A. Aljuhani, D. Javeed, A. Jolfaei, and A. K. M. N. Islam, "Digital twin-driven SDN for smart grid: A deep learning integrated blockchain for cybersecurity," *Sol. Energy*, vol. 263, p. 111921, 2023, https://doi.org/10.1016/j.solener.2023.111921.
[52] N. Qi, K. Huang, Z. Fan, and B. Xu, "Long-term energy management for microgrid with hybrid hydrogen-battery energy storage: A prediction-free coordinated optimization framework," *Appl. Energy*, vol. 377, p. 124485, 2025, https://doi.org/10.1016/j.apenergy.2024.124485.
[53] Alankrita, A. Pati, and N. Adhikary, "Detection and mitigation against false data injection attacks using SHT and ANN in distributed control of DC microgrid," *Electr. Power Syst. Res.*, vol. 241, p. 111356, 2025, https://doi.org/10.1016/j.epsr.2024.111356.